












# Lithogeochemistry and zircon U-Pb geochronology of the Granjeiro Complex and associated units, Curral Novo do Piauí, NW-Borborema Province, Brazil: implications for Archean to Paleoproterozoic crustal evolution

José Alberto Rodrigues do Vale<sup>1\*</sup> , Lena Virginia Soares Monteiro<sup>2</sup> , Camila Franco Basto<sup>3</sup> , Vladimir Cruz de Medeiros<sup>1</sup> , Douglas Almeida Silveira<sup>3</sup> , Evilarde Carvalho Uchôa Filho<sup>4</sup> , Nilo Costa Pedrosa Junior<sup>5</sup> , Joseneusa Brilhante Rodrigues<sup>6</sup> , Ticiano José Saraiva dos Santos<sup>7</sup> 

<sup>1</sup>Serviço Geológico do Brasil-CPRM (NANA/SUREG-RE), Av. Almirante Alexandrino de Alencar, 1402, Natal, RN, Brazil, CEP: 59015-350

<sup>2</sup>Instituto de Geociências, Universidade de São Paulo, Rua do Lago, 562, São Paulo, SP, Brazil, CEP: 05508-080

<sup>3</sup>Serviço Geológico do Brasil-CPRM (SUREG-BH), Av. Brasil, 1731, Belo Horizonte, MG, Brazil, CEP: 30140-002

<sup>4</sup>Serviço Geológico do Brasil-CPRM (REFO), Rua Rodrigues Junior, 840, Fortaleza, CE, Brazil, CEP: 60060-000

<sup>5</sup>Serviço Geológico do Brasil-CPRM (RETE), Rua Goiás, 312, Teresina, PI, Brazil, CEP: 64001-570

<sup>6</sup>Serviço Geológico do Brasil-CPRM (SEDE), Setor Bancário Norte – SBN Quadra 02, Bloco H – Asa Norte, Brasília, DF, Brazil, CEP: 70040-904

<sup>7</sup>Instituto de Geociências, Universidade Estadual de Campinas, Rua Carlos Gomes, 250, Campinas, SP, Brazil, CEP: 13083-855

## Abstract

The Curral Novo Iron District, located in the center-east of the state of Piauí, is hosted in the Granjeiro Complex in its southwestern section, located in the Rio Piranhas-Seridó Domain, northern subprovince of Borborema Province. In this district, the banded iron rocks have an average content of approximately 27% Fe, with an estimated potential of more than one million tons of ore. Through the integration of petrographic, isotopic, geochemical and geochronological field data, a comprehensive characterization of the lithotypes present in the complex (orthogneisses, migmatites and a metavolcano-sedimentary unit) and associated units (syenogranitic orthogneisses and pegmatite granites) was carried out, focusing on the evolutionary discussion of this Archean complex, as well as the origin of metasomatism present in the iron district. Tonalitic and granodioritic orthogneisses include calcic to alkali-calcic rocks with low mafic mineral content. These rocks have low concentrations of lithophile elements and high field potential elements, significant fractionation of light rare earth elements and slightly negative Eu anomalies. U-Pb geochronology in tonalitic orthogneiss zircon from the Granjeiro Complex indicates the age of the protolith in the Paleoproterozoic at 3349 Ma. The metavolcano-sedimentary unit is made up of amphibolites, magnesian schists, serpentinites and banded iron rocks. Such rocks derived from mafic and ultramafic protoliths have a komatiitic and basaltic composition and have a genesis associated with the subduction phase of oceanic plates, presenting a geochemical affinity similar to that of modern island arc rocks. The iron rocks present sedimentary facies of the oxide and silicate types, with strong impoverishment of high field potential elements and rare earth elements and negative Ce anomalies. These units are intruded by syenogranitic plutons, collisional and type A2, aged 2651 Ma. Chemically, these granites are metaluminous to peraluminous, alkali-calcic and ferrous types, having a slight enrichment of light rare earth elements in relation to heavy rare earth elements and high contents of lithophile elements and high field potential elements. The rocks of the Granjeiro Complex show records of strong crustal reworking in the Paleoproterozoic, starting from the Riacian, with a metamorphic peak in metavolcanosedimentary rocks indicated by U-Pb dating in amphibolite zircon at 2200 Ma. An important magmatic event related to the global process of extension of continental masses during the Statherian period, aged 1759 Ma, represented by several intrusive plutons in all units of the area, promoted hydrothermal alteration in the surrounding amphibolites and iron rocks, causing silicification, albitization, potassification, carbonatization, sulfidation and reconcentration of iron.  $\delta^{34}\text{S}$  values = -3.11 to +2.3 per mil in hydrothermal sulfides suggest magmatic sources for the sulfur associated with the hydrothermal system. The incorporation of the analysis of these diverse geological data, made it possible to obtain a detailed understanding of the geological evolution of the Granjeiro Complex in the study area, as well as the origin of metasomatism in the iron district.

## Article Information

Publication type: Research Papers  
Received 15 August 2023  
Accepted 31 October 2023  
Online pub. 22 November 2023  
Editor: E. Klein

### Keywords:

Curral Novo Iron District,  
Borborema - Northern Subprovince,  
U-Pb Geochronology in zircon,  
Crustal Evolution,  
Iron ore

### \*Corresponding author

José Alberto Rodrigues do Vale  
E-mail address: [jose.vale@sgb.com.br](mailto:jose.vale@sgb.com.br)

## 1. Introduction

The area of the Curral Novo do Piauí Iron District (CNPID) is located in the Northern Subprovince of the Borborema Province

(Almeida et al. 1981; Brito Neves et al. 2000), forming part of the so-called Granjeiro Complex (Fig 1). DFCNP is located on the outskirts of the municipality of Curral Novo do Piauí, located 459 km from Teresina – State of Piauí, and 230 km from the



municipality of Petrolina – State of Pernambuco. Access to the area is via the BR-316 highway from Teresina or following the BR - 407 and transiting to PI -142 and PI – 456, starting in Petrolina. Cartographically, the work was developed in the central-southern portion of Folha Simões (SB.24-YC-VI), within the following geographic limits: 7°45'S and 40°30'W; 7°45'S and 41°0'W; 8°0'S and 40°30'W; 8°0'S and 41° 0'W (Fig. 2).

The Granjeiro Complex, of Archean age, comprises migmatized orthogneisses and a metavolcano-sedimentary unit, composed of magnesian schists, amphibolites, quartzites and banded iron rocks (Silva et al. 1997; Vasconcelos and Gomes 1998; Freimann 2014; Ancelmi 2016; Martins 2017; Pitarello et al. 2019; Gomes et al. 2021).

At CNPID, located near the municipality of Curral Novo do Piauí, state of Piauí, the ore is hosted in a metavolcanosedimentary unit (Sato 2011; Santos et al. 2014). The banded iron rocks are distributed in elongated bodies, kilometeric in length, affected by shear zones, whose

deformation effects generate bodies of banded ore with a high dip angle.

The rocks of the Granjeiro Complex in the CNPID region underwent significant hydrothermal alteration, the origin of which was previously interpreted as the result of fluid-rock interaction involving magmatic fluids exsolved during the emplacement of granitoids in the Neoproterozoic (Santos et al. 2014). According to Santos et al. (2014), the hydrothermal process caused the reconcentration of iron in the deposit, in addition to intense chemical modification of the host rocks, with enrichment of elements such as Si, K, ETRL, Th, Ta, U, Zr, Y, Cu, Zn and B. This process was considered a critical factor for the enrichment of iron in portions of the district, in targets that reach grades of around 40% Fe.

This study aims to enrich the geological understanding of the Granjeiro Complex, as well as the CNPID. This is achieved through the proposition of a crustal evolutionary model, which is based on the introduction of new geological data covering

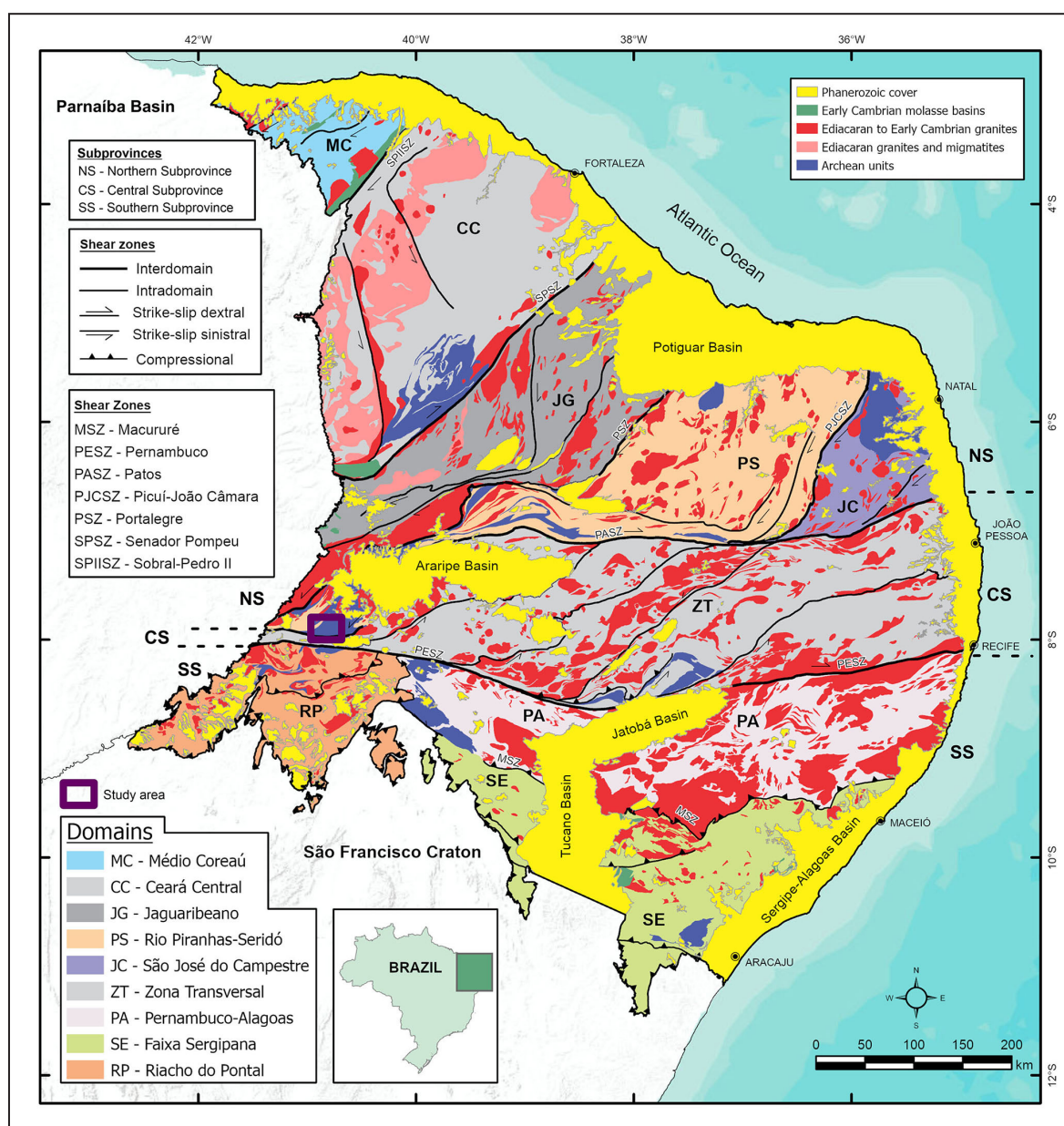


**FIGURE 1.** Tectonic framework of the Borborema Province and its division into North, Central (or Transversal) and South subprovinces, in addition to their respective domains (Medeiros et al. 2021).

the main lithostratigraphic units that make up the Granjeiro Complex and associated units. Thus, new petrographic, geochemical and geochronological information is provided regarding the granodioritic and tonalitic orthogneisses, as well as the metamafic, metaultramafic and banded iron rocks of the metavolcano-sedimentary unit. Additionally, the associated units are characterized: syenite orthogneisses and pegmatite plutonic bodies, the latter associated with the potential source of fluids responsible for the hydrothermal process in the CNPID.

## 2. Geological framework

The Borborema Province, located in Northeast Brazil, consolidated during the Brasiliano orogenic event, defined as part of the Neoproterozoic collage of Western Gondwana, corresponding to the collision of a complex orogenic system located between the São Francisco-Congo and São Luis-West Africa cratons (Almeida et al. 1981; Jardim de Sá 1994; Brito Neves et al. 2000; Van Schmus et al. 2008). This province comprises domains with intricate geological evolution, composed of Archean cores bordered by Proterozoic bands

originating from the formation of the Paleoproterozoic supercontinent Columbia. Subsequently, the Archean-Paleoproterozoic basement was overprinted by Meso- and Neoproterozoic supracrustal associations and intruded by Neoproterozoic granitoids (Van Schmus et al. 2008; Araujo et al. 2012; Caxito et al. 2021; Pinéo et al. 2023).

The Province's compartmentalization is commonly divided into the following sub-provinces: North Subprovince, with its lower limit defined by the Patos Lineament; Central Subprovince or Transversal Zone, limited to the south by the Pernambuco Lineament and to the north by the Patos Lineament; and Southern Subprovince, overlapping the São Francisco Cráton through areas of thrust faults (Brito Neves et al. 2000; Delgado et al. 2003; Oliveira et al. 2023; Fig. 1).

The Northern Subprovince consists of five distinct tectonic domains, limited by dextral shear zones, namely: Middle Coreau Domain (or NW of Ceará), Central Ceará Domain, Jaguaribeano Domain; Domain Rio Piranhas-Seridó and Domain São José do Campestre (Medeiros et al. 2021). The study area, where the Granjeiro Complex is located, is located within the Rio Piranhas-Seridó Domain.

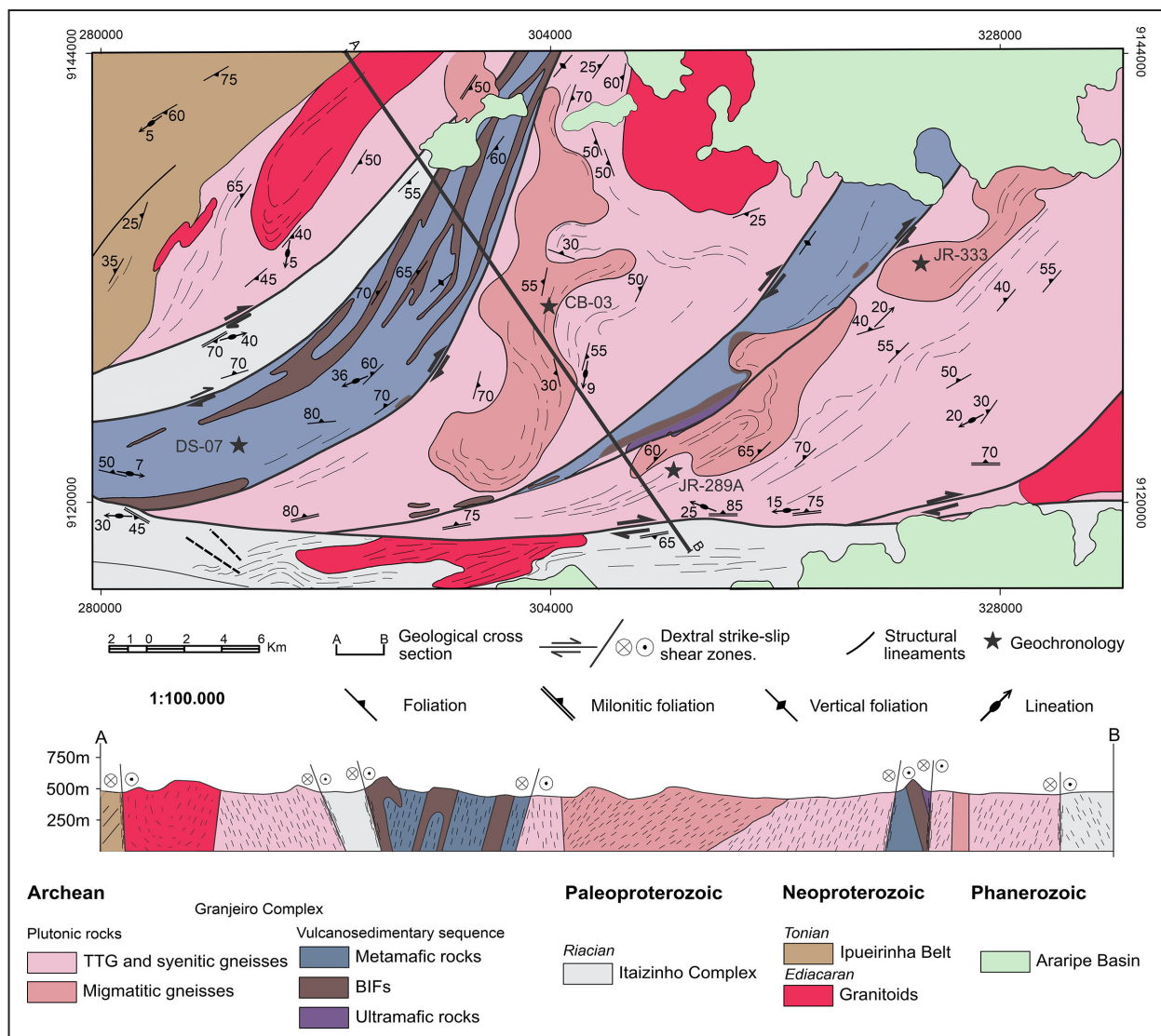


FIGURE 2. Simplified geological map of the area of the iron district of Curral Novo-PI, central-south portion of Folha Simões (Uchôa Filho et al. 2019).



## 2.1. Archean Nuclei from the Rio Piranhas-Seridó Domain

The Rio Piranhas-Seridó Domain contains small Archean cores composed of migmatitic orthogneisses, metamafic and metaultramafic rocks, banded iron rocks and metasedimentary rocks consisting of quartzites, marbles and paragneisses, distributed in the following complexes: Amarante (3.74 to 3.34 Ga), Granjeiro (3.53 to 2.54 Ga), São José do Campestre (3.41 to 2.65 Ga), Campo Grande (2.69 to 2.65 Ga), Saquinho (2.51 to 2.50 Ga) and the Serra do Ingá Unit (2.67 Ga) (Silva et al. 1997; Jesus 2011; Dantas et al. 2013; Martins 2017; Souza et al. 2016; Cavalcante et al. 2018; Dantas et al. 2019; Pitarello et al. 2019; Ruiz et al. 2019; Santos et al. 2020; Gomes et al. 2021).

## 2.2. Granjeiro Complex

The Granjeiro Complex occurs in the form of an extensive sigmoidal structure, along a continuous belt of predominantly E-W direction in the central-western portion of the Rio Piranhas-Seridó Domain, flexing to the SW in the lower portion of this domain (Angelim et al. 2004; Santos et al. 2021). Geographically, it comprises two distinct regions of occurrence, the first being in the south of the state of Ceará (northeast portion of the complex) and the second in the southeast of the state of Piauí (southwest portion of the complex). The continuity of the Granjeiro Complex is covered by the sedimentary rocks of the Araripe Basin, however its continuity in the subsurface follows the inflection of the Patos Lineament to the south.

The Granjeiro Complex in the area of this study is composed of two distinct units, the first being represented by a metaplutonic association of tonalitic-granodioritic composition, with a subordinate presence of trondhjemitic gneisses, with an alkaline lineage and mantle derivation (Silva et al. 1997; Vasconcelos and Gomes 1998). Along with this association, there are migmatite gneisses, granitic and syenitic orthogneisses, as well as pegmatitic granitic bodies. The metavolcanosedimentary unit constitutes a lithological group formed by amphibolites, metatuffs, metaultramafic rocks, schists and calciosilicates, metalimestones, quartzites, banded iron rocks and metacherts (Vasconcelos and Gomes 1998; Gomes and Vasconcelos 2000).

The evolution of geological knowledge about the Granjeiro Complex reflects a continuous process of data collection over the years, allowing the construction of models in relation to its genesis, with the northeastern portion of the Complex being the most studied. Previous studies conducted by Campos et al. (1976) and Prado et al. (1980) initially considered this complex as an integral part of the Archean basement, correlating it, at the time, with the Caicó Complex, within the Rio Piranhas-Seridó Domain). Ribeiro and Vasconcelos (1991) conducted geological mapping at the 1:100,000 scale of Folha Simões, defining the basement units as the Lower Unit. Silva (1993), based on petrographic and geochemical data, identified the unit as the Granjeiro Complex. Subsequently, Silva et al. (1997) conducted the first U-Pb SHRIMP dating in zircon in the orthogneisses of the Complex in the region of Granjeiro - Ceará, obtaining an age of 2.54 Ga, which defined the Complex as belonging to the Archean. The metavolcanosedimentary association was interpreted by Vasconcelos and Gomes (1998) as evidence of the formation of oceanic crust

and the development of exhalative horizons. Based on model ages in the range 2.65 to 2.55 Ga obtained from orthoderived rocks, Fetter (1999) suggested that this area could represent a juvenile terrane remnant of a possible magmatic arc-ocean basin system.

Bautista (2012) presented model ages  $T_{DM}$  situated in the range of 2.70 to 2.60 Ga for orthogneisses, while the U-Pb crystallization ages in zircon define a range ranging from 3.10 to 2.35 Ga, including in this result the amphibolite age. Freimann (2014) introduced new geochronological data using U-Pb via LA-ICP-MS in the northeastern portion of the Granjeiro Complex. These data provided an age of 3.2 Ga for a biotite gneiss and 3.0 Ga for an ultramafic rock from the Complex's metavolcanosedimentary association. Ancelmi (2016), in his geochemical and geochronological study of the Granjeiro Nordeste Complex, proposed a tectonic model for the Granjeiro Complex, in which the metavolcanosedimentary association originated in a basin of back arc through a subduction system, generating a continental magmatic arc around 2.7 to 2.6 Ga. This is based on U-Pb LA-ICP-MS ages in zircon ranging between 2.7 to 2.6 Ga for amphibolites and ultramafic rock from the aforementioned unit. Furthermore, this system may have been simultaneously influenced by mantle plumes, which contributed to the formation of ultramafic magmas with a komatiite composition. The author also dated orthogneisses of intrusive quartz-dioritic and granodioritic composition, obtaining ages between 2.49 and 2.46 Ga, and migmatized rocks of granitic composition, with U-Pb ages in zircon (LA-ICP-MS) between 2.17 and 2.16 Ga. Ancelmi (2016) interpreted this Rhyacian unit as juvenile rocks reworked during the process of continental collision with Archean microplates.

Gomes et al. (2021) provided updated U-Pb SHRIMP dating data on zircon for the Granjeiro Complex, obtaining an age of 3.00 Ga for orthogneiss and 2.76 Ga for amphibolite. Furthermore, Archanjo et al. (2021) performed dates on banded gneisses belonging to the Complex, obtaining ages of 3.0 and 2.7 Ga. Additionally, dating of migmatite gneisses and metatextites revealed ages corresponding to the Siderian and Rhyacian periods, covering the interval from 2.4 to 2.1 Ga.

In the southwestern portion of the Granjeiro Complex, the work of Martins (2017), Pitarello et al. (2019) and Brito Neves et al. (2022). The first author reported dates on tonalitic and syenogranitic orthogneisses, obtaining ages of 3.42 and 2.66 Ga, respectively. The second study presented U-Pb dating in zircon, via LA-ICP-MS, in granodioritic and tonalitic orthogneisses (3.53 to 2.72 Ga) and metamafic rocks (2.75 to 2.65 Ga). In addition, the study also investigated the iron rocks in the region. The mineralogical and geochemical patterns observed suggest a subdivision into three distinct groups: deposition of chemical sediments from seawater in regions further away from the continent, with a low influx of terrigenous sediments; deposition close to the continent; and chemical sediments precipitated from seawater with post-depositional or hydrothermal alteration processes. Brito Neves et al. (2022) carried out a series of geochronological dates using the Sm-Nd and U-Pb method on the lyotypes that make up the complex. The results revealed TDM values varying between 2.29 and 3.48 Ga, and  $\epsilon_{Nd}$  values situated between -22.64 and -43.78, indicating sources in the interval between the Paleoproterozoic and Paleoarchean for these units. The U-Pb Ages obtained for different orthogneisses comprised an



age range between 3.5 and 2.3 Ga. Based on this information, Brito Neves et al. (2022) suggest that the region in which the Granjeiro Complex is located, called São Pedro Terrain in this study, may represent an extension of the Gavião Block, the northern portion of the São Francisco Cráton.

Given this, it becomes evident that the Granjeiro Complex covers an extensive geological period, stretching from the Archean to the Paleoproterozoic. It is possible to organize these ages into distinct geological intervals, such as Paleoarchean (3.5 to 3.3 Ga), Mesoarchean (3.1 to 3.0 Ga), Neoarchean (2.7 to 2.5 Ga) and Paleoproterozoic (2.4 Ga and 2.2 to 2.1 Ga). These intervals will be discussed in detail throughout this work, together with new data presented, which facilitates the understanding of the different stages of the geological evolution of the complex and the relationships between events over time.

### 3. Materials and methods

Geological mapping was carried out by the Geological Survey of Brazil (SGB) at a scale of 1:100,000 in the central-southern portion of Folha Simões (Uchôa Filho et al. 2019), where Piauí's CNPID is located. In this work, representative samples of outcrops and drilling cores were collected. The petrographic characterization occurred through the petrographic analysis of 72 thin sections and 40 polished sections conducted by the Mineral Analysis Laboratory (LAMIN) of the Teresina Residence (RETE) of the Geological Survey of Brazil and by the Geosciences Institute of the University of São Paulo (IG-USP), respectively.

The lithochemical analysis of 54 samples was carried out by Geosol laboratories using the ICP-MS (Inductively Coupled Plasma Mass Spectrometry) analytical technique for trace elements and rare earths. The Loss on Ignition (LOI) was determined by the difference in weight after heating at 450°C and/or 1000°C.

Geochronological analysis of zircon by the U-Pb LA-ICP-MS method (Laser Ablation Inductively Coupled Plasma Mass Spectrometry) were carried out at the Analytical Center (CA), Geochronological Research Center (CPGeo) and Isotopic Geology Laboratory (LAGIS), of the Federal University of Ouro Preto (UFOP), University of São Paulo (USP) and University of Campinas (UNICAMP), respectively. At UFOP (CA), U-Pb analysis were carried out using the Pothon-Machines 193 nm G2 laser system coupled to the Thermo-Finnigan Neptune multicollector LA-MC-ICP-MS (Laser Ablation Multi Collector Inductively Coupled Plasma Mass Spectrometer), following the procedures described in Santos et al. (2017). The instrument configuration parameters covered spots with a size of 20 µm, a frequency of 6 Hz and 10% energy with an intensity of 0.3 mJ. The U-Pb data were standardized using GJ-1 zircon (reference age  $608.5 \pm 0.4$  Ma; Jackson et al. 2004) as the primary standard, and tested using Pleisovice zircon (reference age  $337.13 \pm 0.37$  Ma, Sláma et al. 2008) as a secondary standard. External errors were propagated by considering the internal reproducibility of individual ratios, external reproducibility of GJ-1, the long-term uncertainty of the validation material, the uncertainties of the reference material, and the uncertainty of the Pb-common ratio (Lana et al. 2017).

At USP (CPGeo), U-Pb isotope analysis were carried out using the equipment Thermo Neptune laser ablation multicollector inductively coupled plasma mass spectrometer (LA-

MC-ICP-MS) with special analytical resolution obtained by the 193 nm ArF Excimer Laser (6Hz frequency), producing 32 µm spots and 40s ablation time. The analytical procedure followed that presented by Sato et al. (2008). The correction for common Pb was based on GJ-1 zircon. At UNICAMP (LAGIS), the equipment used was the Photon Machine Excimer 193 system with HelEx ablation cell, attached to the Thermo Scientific Element XR ICP-MS, with the following characteristics: laser beam diameter of 25 µm, repetition rate of 10 Hz and fluence of 4.74 J/cm<sup>2</sup>. In the equipment's analytical procedures, standard zircon 91500 was used (Wiedenbeck et al. 1995). The method involved the subtraction of white gas followed by correction of the downhole fractionation, compared to the 91500 standard. Correction of raw data included equipment bias, exclusion of analysis with high common Pb values, and consideration of analysis with U (ppm) values < 500, values of  $f_{206} < 1$  and ratio  $^{206}\text{Pb} / ^{204}\text{Pb} > 10,000$ . Data reduction was carried out using the software - Vizual Age (Petrus and Kamber 2012) from the IOLITE package (Paton et al. 2010) and the ISOPLOT/EX 4.15 software (Ludwig 2009).

The analysis of stable sulfur isotopes was carried out at the Geochronology Laboratory of the Institute of Geosciences, University of Brasília. Five pyrite concentrates with purity greater than 95% were obtained using a manual drill and subsequent screening under a stereomicroscope. For analysis of sulfur isotopes, the production of SO<sub>2</sub> was obtained from the combustion of sulfides with excess oxygen in tin capsules at 1080°C. The gas produced by combustion was taken from a helium stream to tungsten and zirconium catalysts for reduction into high-purity copper filament. The separation of the OS<sub>2</sub> occurred in a gas chromatograph. Stable isotope ratios were analyzed using the Neptune MC-ICP-MS coupled to a NewWave UP213 Nd:YAG ablation source for solid sample analysis, employing the procedures described by Craddock et al. (2008). Data processing, as well as control of the mass spectrometer and its peripherals, were performed using the Isodat 3.0 software. The values of δ<sup>34</sup>S have an accuracy of 0.01‰ and have been reported to the Vienna Canyon Diablo Troilite (V-CDT) standard.

### 4. Geology of the study area

In the Curral Novo Iron District, the Granjeiro Complex represents the main geological unit, comprising granodioritic, tonalitic orthogneisses, sometimes migmatized, and a metavolcanic-sedimentary association, composed of plutonic and volcanic metamafic rocks (metagabbros and amphibolites), magnesian schists, serpentinites, quartzites and banded iron rocks. These units are transposed by shear zones with a NE-SW structural pattern and high-angle dips, flexing to the E-W, parallel to the Patos Lineament.

In the district region, the Granjeiro Complex lithotypes are intruded by syenogranitic, syenitic and pegmatite granite plutons, which are not cartographically individualized at the mapping scale. The study area covers the delimitation of the Granjeiro Complex to the north, where the Ediacaran metasedimentary rocks of the Ipueirinha Group are found, and to the south, by the Itaizinho Complex, composed of migmatitic orthogneisses and associated supracrustal rocks, in contact defined by the Patos Lineament. These lithostratigraphic units are covered by Phanerozoic sedimentary rocks from the Araripe Basin (Fig. 2).

Granodioritic and tonalitic orthogneisses are the most representative lithotypes of the Granjeiro Complex (Fig. 3A). They are gray in color, fine to medium grained (arising from mylonitization), have a characteristic gneiss banding and have a mylonitic structure close to the shear zones. In addition to the mylonite foliation, ribbon quartz, porphyroclasts, pressure shadows and SC structures indicate dextral kinematics, consistent with the regional structuring of the area. Sometimes, the mylonitic foliation is crenulated, exhibiting asymmetric microfolds with an axis in the NE direction and vergence towards the south. The gneiss band is centimeter thick, with alternating felsic bands, composed by quartz, plagioclase and subordinate alkali feldspar, and mafic bands formed by biotite, amphibole, epidote, and subordinate pyroxene.

Migmatite orthogneisses are well-defined bodies on the geological map, resulting from anatexis caused by metamorphism in the lithotypes of the Granjeiro Complex (Fig. 3B). Structurally, they may present crenulation and development of foliation parallel to the banding, in addition to isoclinal and recumbent folds. Orthogneisses are identified as metatextites, according to Brown's (1973) classification, highlighting stromatic or net-veined, with distinction from the leucosome, melanosome and paleosome. The leucosome is composed mainly of alkali feldspar and quartz. The mesosome presents biotite, quartz, plagioclase and alkali feldspar and the melanosome is represented mainly by concentrations of biotite that occur as remnants at the edges of the leucosome, indicating anatexis in situ.

The rocks of the metavolcano-sedimentary association occur in parallel or discordant contacts with orthogneisses. Amphibolites (basaltic protolith) are fine-grained and greenish-gray in color (Fig. 3C). Its mineralogy mainly includes plagioclase and hornblende, which define a nematoblastic texture. Hydrothermal mineral phases include biotite (potassium alteration), epidote, chlorite, sulfides (pyrite, chalcopyrite and pyrrhotite) and magnetite, with the occurrence of quartz and carbonate veins in a late phase. The metagabbros (Fig. 3D) are coarse-grained and have a nematoblastic texture, with relicts of igneous augite, and a metamorphic association consisting mainly of hornblende and plagioclase, with actinolite, chlorite and epidote related to retrometamorphic transformations.

Metaultramafic rocks are represented by magnesian schists and serpentinites, generally interspersed with metamafic bodies. Magnesian schists have fine grain and lepidonematoblastic texture, crenulation and mineralogical constitution comprising tremolite, chlorite, talc and magnetite. Serpentinites have a lepidoblastic texture and contain antigorite-type serpentine as their main constituent, in addition to chlorite, tremolite, talc and clinocllore as subordinate minerals.

Quartzites are closely related to banded iron rocks and metamafic rocks, interspersed with them. They are foliated rocks, due to the presence of mica, with layers that vary in thickness from millimeters to decimeters. Its main composition includes quartz and micas (muscovite and fuchsite) with a whitish and greenish color, or reddish, due to iron oxidation.

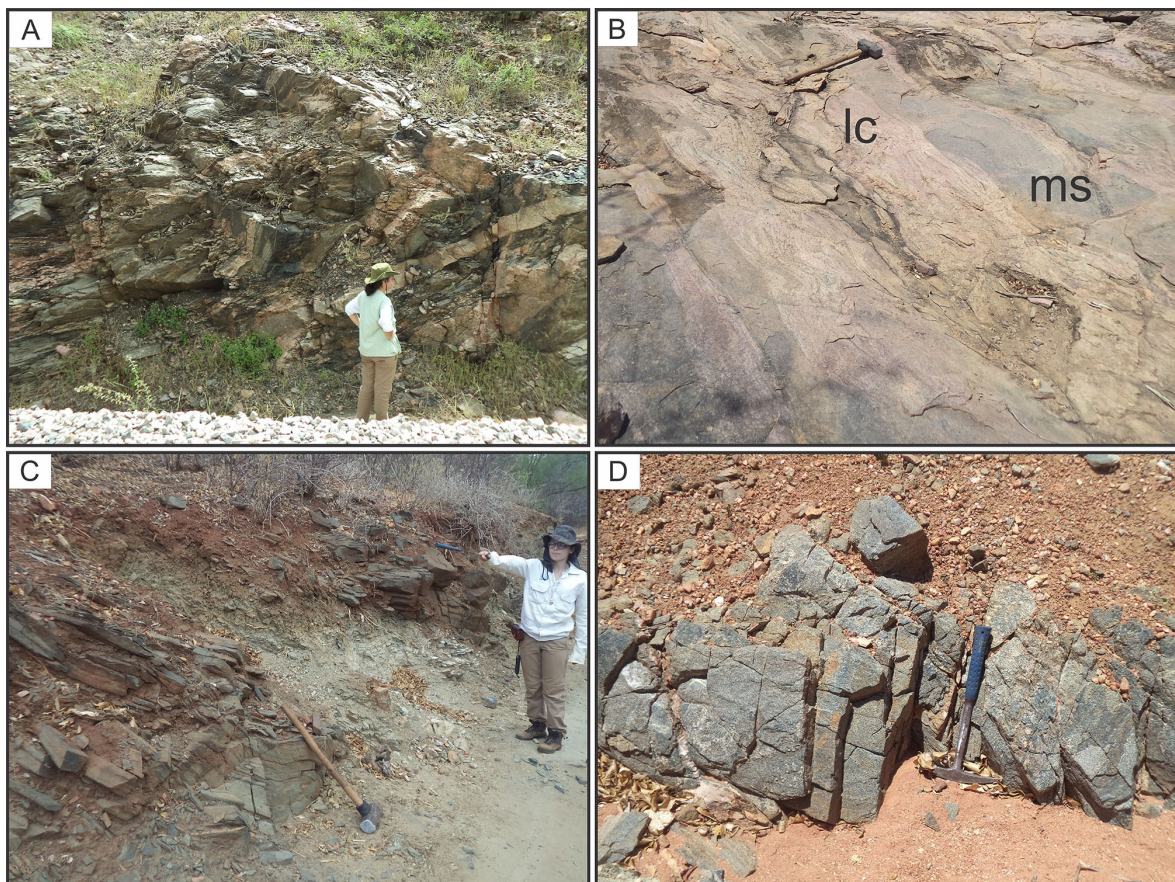


**FIGURE 3.** (A) Outcrop of tonalitic orthogneiss, located close to the Patos shear zone (DS-R-13); (B) Outcrop of migmatitic orthogneiss, highlighting the gray mesosome (ms) and pinkish leucosome (lc) (CB-R-03); (C) Outcrop of amphibolite derived from basaltic volcanic protolith of the Granjeiro Complex (DS-R-10); (D) Detail of the metagabbro body (JR-R-316A).



Banded iron rocks (RFBs) crop out mainly in aligned hills that follow the NE-SW regional structure, a pattern defined by regional foliation, and can be easily visualized in the field and in drilling cores. The bodies have a NE direction and a high dip angle to the SE, above 45°, being predominantly subvertical close to the shear zones. Intense shear also results in transposition of the band and formation of tight or isoclinal, sheathed, and parasitic folds. In general, iron rocks are greenish gray when preserved and reddish brown when weathered, with grains varying from fine to coarse and bands of millimeter to centimeter thickness, characterized by the alternation of silicate and oxide minerals (Fig. 4A and B). The silicate facies is composed of quartz and amphiboles, of the types grunerite, actinolite and hornblende, in addition to chlorite subordinately. The oxide facies comprises magnetite with a variable degree of alteration to hematite and goethite. Quartz and carbonate veins are present, with reconcentration and recrystallization of magnetite close to the intrusion of pegmatite bodies, which is indicative of hydrothermal activity affecting these iron rocks.

The syenogranitic orthogneisses (Fig. 4C) have a pink color and medium to coarse grain, presenting a porphyroclastic texture with a mylonitic matrix, with a percentage of 50% of the matrix characterizing protomylonites, the result of comminution and dynamic recrystallization processes.

Finally, metavolcano-sedimentary rocks and granodioritic, tonalitic and syenogranitic orthogneisses are intruded by pegmatite bodies (Fig. 4D). The main constituent minerals are

quartz and alkali feldspar, with plagioclase being subordinate. Alkaline feldspar grains can be decimeter-sized. The contacts of pegmatites in outcrop and drill core cause metasomatism, mainly potassic zoning, in the vicinity of the intrusions. When intrusive in RFBs, it generates hydrothermal remobilization of iron and crystallization of hydrothermal magnetite, which occurs dispersed or in concentrations.

## 5. Hydrothermal alteration

The intrusive pegmatite granite bodies in the Granjeiro Complex lithotypes are responsible for hydrothermal alteration processes recorded in these units. The types identified were: silicification; garnet-muscovite association; albitization; potassium alteration; carbonation; sulfidation and sericitization, described below.

(a) Silicification – Incipient to intense, pervasive silicification is common in syenogranitic and amphibolite orthogneisses. Quartz replaces feldspar porphyroclasts, obliterating the original texture of orthogneisses (Fig. 5A). Its crystals present wavy extinction, straight or serrated contacts, formation of subgrains, banded quartz and deformation bands. (b) Formation of garnet and muscovite – In zones of deformation in syenogranitic orthogneisses and pegmatite bodies, the formation of interstitial crystals of garnet and muscovite occurs (Fig. 5B). The strong leaching of alkaline content and the relative increase in the Al content of the system may be associated with this process. (c) Albitization – The formation

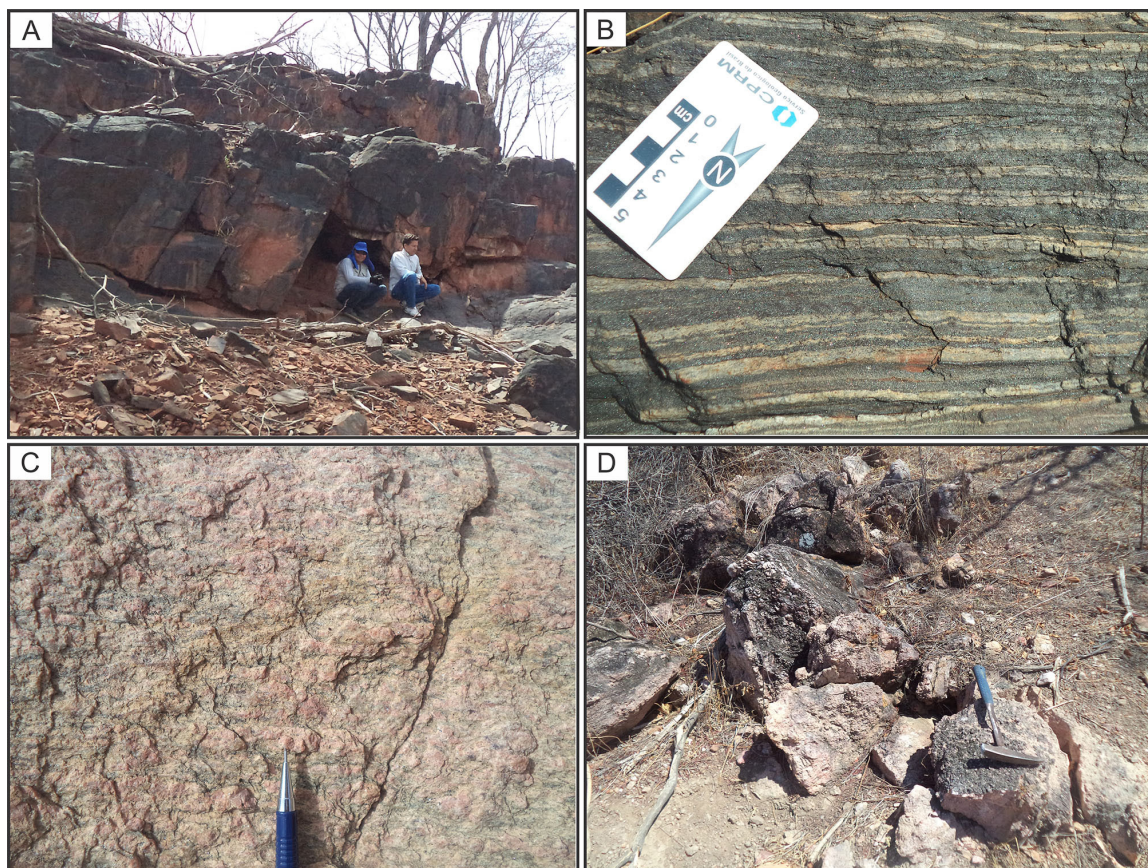


**FIGURE 4.** (A) General aspect of the banded iron rock outcrop of the Granjeiro Complex (JR-R-334); (B) Detail of the banding in iron rocks banded in alternation of silicates (quartz + grunerite) and oxide (magnetite) (JR-R-323); (C) Detail of the syenitic orthogneisses and their significant presence of alkali feldspar (JR-R-297); (D) Pegmatite intrusion in amphibolite from the Granjeiro Complex (CB-R-14).



of albite characterizes this stage of alteration in which it occurs mainly as fine crystals on the edges of deformed feldspar porphyroclasts in syenogranitic orthogneisses and pegmatites. It is common in neofomed albite to have the chessboard texture. Scapolite also replaces plagioclase in these rocks, characterizing sodic metasomatism. (d) Potassium alteration – most striking in orthogneisses. Potassium feldspar replaces feldspar porphyroclasts along microfractures and at the edges. Locally, hydrothermal potassium feldspar completely replaces gneiss feldspar, resulting in new crystals with a cloudy appearance. Biotite crystals form changes in the amphibole, at its edges or through overgrowth. The formation of magnetite in syenogranitic orthogneisses is associated with potassic alteration, resulting in the mineral association potassium feldspar-biotite-magnetite (Fig. 5C and D). (e) Carbonation – Occurs at a late stage, but associated with brittle-ductile deformation, present in all lithotypes of the metavolcanosedimentary unit. Veins filled with calcite accompany the mylonitic foliation. Also, there is an occurrence of carbonates in breccias (Fig. 6A and B). The most intense alteration process involves pervasive alteration with the replacement of hornblende crystals by calcite. (f) Sulfidation – The formation of these minerals in amphibolite rocks represents late stages of hydrothermal activity. Sulfides represented by pyrite,

chalcopyrite and pyrrhotite commonly occur at the edges of garnet and magnetite, but also, filling fractures and in the breccia matrix associated with brittle-ductile structures (Fig. 6C and D). (g) Sericitization – last phase, occurs mainly in plagioclase porphyroclasts in orthogneisses, which can be completely replaced by sericite and epidote. In this case, the final product of this hydrothermal process is the sericite-(muscovite)-epidote association.

## 6. Lithochemistry

### 6.1. Granodioritic and tonalitic orthogneisses

The ten samples selected for lithochemical studies of orthogneisses of tonalitic and granodioritic composition are presented in Appendix 1, and show variation in  $\text{SiO}_2$  content between 63.51 and 71.16%, with high values of  $\text{Na}_2\text{O}$  (2.6 to 4.8%) and  $\text{Al}_2\text{O}_3$  (11 to 16%), moderate  $\text{K}_2\text{O}$  content (2.3 to 5.4%) and  $\text{CaO}$  (0.8 to 3%) and low concentration of  $\text{MgO}$ ,  $\text{P}_2\text{O}_5$ ,  $\text{TiO}_2$  and  $\text{MnO}$ . The reason  $\text{Na}_2\text{O}/\text{K}_2\text{O}$  varies between 0.5 and 2.

The ternary diagram  $\text{Al}_2\text{O}_3/(\text{FeO} + \text{MgO})$  vs.  $3\text{CaO}$  vs.  $5(\text{Na}_2\text{O}/\text{K}_2\text{O})$  proposed by Laurent et al. (2014) was used to discriminate different types of Archean granitoids according to the petrogenetic process of origin (Fig. 7A). In this way,

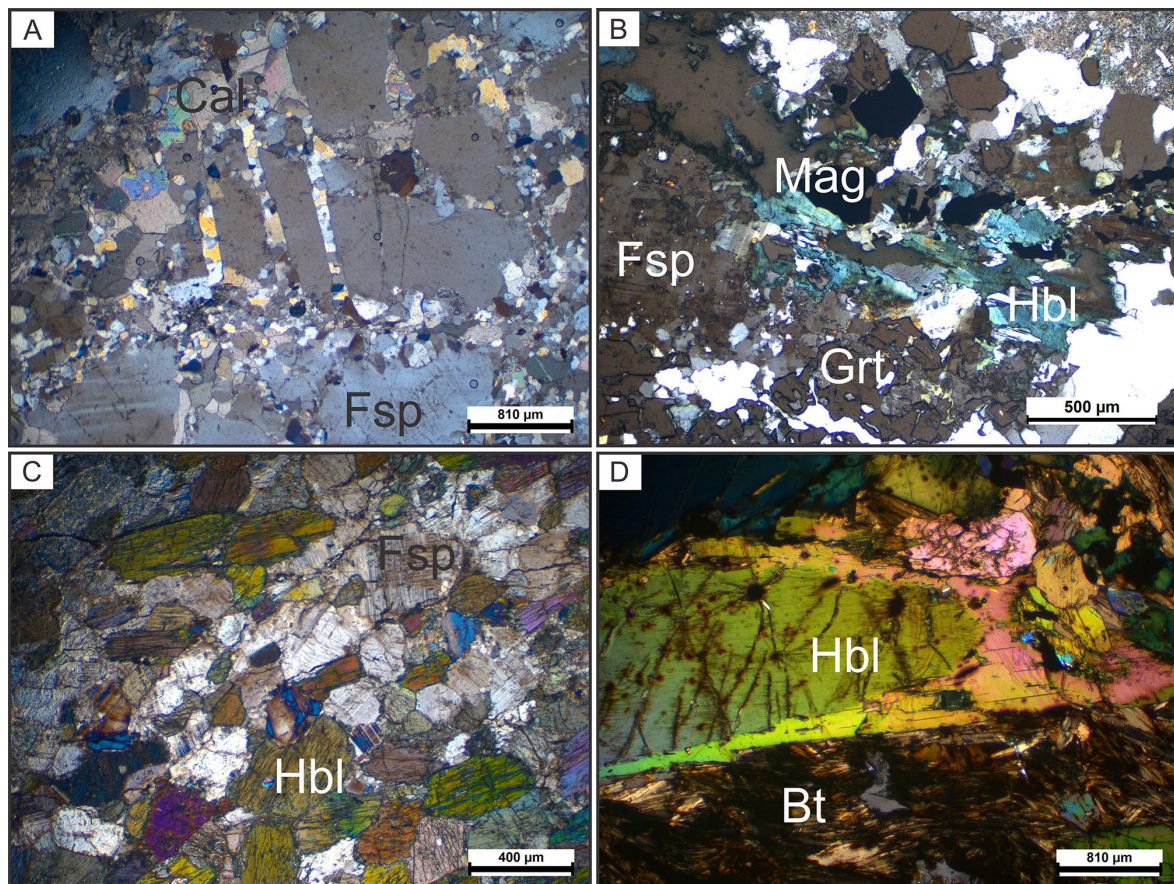


**FIGURE 5.** (A) Potassic feldspar (Fsp) pseudomorphs fractured and completely replaced by quartz associated with calcite (Cal). Transmitted light (JR-R-341I); (B) Replacement of potassium feldspar (Fsp) and hornblende (Hbl) by garnet (Grt) and magnetite (Mag). Transmitted light, crossed polarizers (JR-R-342A); (C) Potassium alteration, represented by the crystallization of potassium feldspar (Fsp) in amphibole-rich metamafic (Hbl). Transmitted light, crossed polarizers (JR-R-324B); (D) Photomicrograph of metamafic rock (amphibolite) with hornblende (Hbl) crystals replaced by biotite (Bt) in its interstices. Transmitted light, crossed polarizers (JR-R-345E). Mineral abbreviations according to Whitney and Evans (2010).



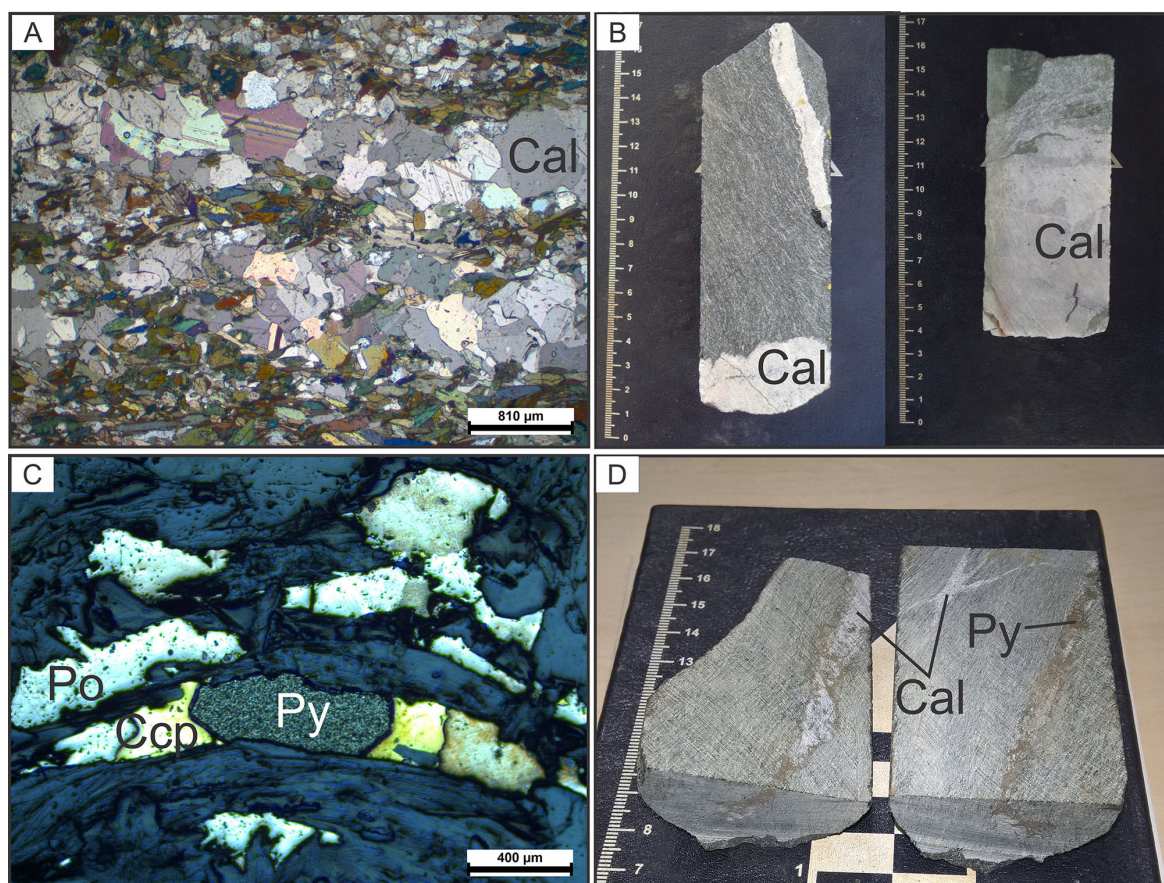


**FIGURE 6.** (A) Carbonatization in amphibolites with calcite (Cal) accompanying the foliation. Transmitted light, crossed polarizers; (B) Calcite vein (Cal) and zones of pervasive carbonate alteration; (C) Photomicrograph with sequential crystallization of sulfides, initially forming pyrite (Py), transitioning to chalcocopyrite (Ccp) and pyrrhotite (Po). Reflected light; (D) Pyrite (Py) and calcite (Cal) veins in amphibolite samples from drill cores. Mineral abbreviations according to Whitney and Evans (2010).

there is a transition in the classification of the study samples between the biotite-bearing granites and sanukitoid rocks. In the diagram in Figure 7B (Laurent et al. 2014) the gneiss samples are mainly located in the field of high-K mafic rocks.

The diagram  $\text{Na}_2\text{O} + \text{K}_2\text{O} - \text{CaO}$  (wt. %) vs.  $\text{SiO}_2$  by Frost et al. (2001) indicates alkali-calcic to calcic-alkaline affinity (Fig. 7C) and, in the binary diagram  $\text{SiO}_2$  vs.  $\text{FeO}/(\text{FeO} + \text{MgO})$ , the samples are located close to the threshold of ferrous to magnesian composition, with the latter predominating (Fig. 7D).

Orthogneisses show considerable variation in  $\Sigma\text{ETR}$  values, ranging between 70 and 836 ppm. Europium anomaly values ( $\text{Eu}/\text{Eu}^* = 0.4$  to 1.9) correspond to positive or negative values. The ratio  $(\text{La}/\text{Yb})_N$  varies between approximately 10 to 140 and reveals strong fractionation of ETRL (light rare earth elements) over ETRP (heavy rare earth elements), a pattern that also repeats when the rare earth elements are normalized to chondrite (Boynton 1984; Fig. 8A). The distribution patterns of trace elements (Fig. 8B) normalized to the primitive mantle (McDonough and Sun 1995) show more significant negative anomalies for P and Ti and lower intensity for the elements Nb and Ta. In contrast, they are enriched in some elements with high crustal affinity, such as Th, Pb, U, Cs and Rb.

Figures 9A and 9B show the correlation between trace elements in the Y vs. Y diagrams. Sr/Y and Yb vs. La/Yb, whose values are inversely proportional to the concentrations present in the samples. The tectonic discrimination diagram of Pearce (1996) shows that the chemical signatures of the

studied gneisses are similar to those originating in magmatic arcs, with three samples positioned in the intraplate granitoid field (Fig. 9C). Finally, in the diagram Sr vs. Y, by Moyen (2011), which correlates the ratio of these elements with pressure environments, relative to the depth of magma generation, the samples are dispersed across the three pressure spectra in the magma generation environments (Fig. 9D).

## 6.2. Syenogranitic orthogneisses

The four samples of syenogranitic gneisses have high  $\text{SiO}_2$  content (69 to 78%), alkalis ( $\text{Na}_2\text{O} = 2.5$  to 6.5%;  $\text{K}_2\text{O} = 1.7$  to 6.6%) and  $\text{Al}_2\text{O}_3$  (12 to 17.8%) and low concentration of the elements CaO, MgO,  $\text{P}_2\text{O}_5$ ,  $\text{TiO}_2$  and MnO (Appendix 2). There is a subtle difference in  $\text{K}_2\text{O}$  levels relative to  $\text{Na}_2\text{O}$  if there is a ratio in the median  $\text{Na}_2\text{O}/\text{K}_2\text{O} < 1$  (0.96).

The classification based on the A/CNK – A/NK diagram (Shand 1943) indicates metaluminous to peraluminous composition (Fig. 10A) and, according to the diagram  $\text{Na}_2\text{O} + \text{K}_2\text{O} + \text{CaO}$  (wt. %) vs.  $\text{SiO}_2$  (wt. %) by Frost et al. (2001; Fig. 10B), such samples are mainly located in the field of alkalic-calcic rocks. The high  $\text{FeOt}/(\text{FeOt} + \text{MgO})$  ratios, varying between 0.8 and 2, indicate ferrous composition (Fig. 10C) in the diagram  $\text{FeOt}/(\text{FeOt} + \text{MgO})$  vs.  $\text{SiO}_2$  by Frost et al. (2001).

Syenogranitic gneisses have  $\Sigma\text{ETR}$  values between 228 and 563 ppm.  $\text{Eu}/\text{Eu}^*$  values (0.19 to 0.57) indicate strong negative Eu anomalies. The ratio  $(\text{La}/\text{Yb})_N$  varies between

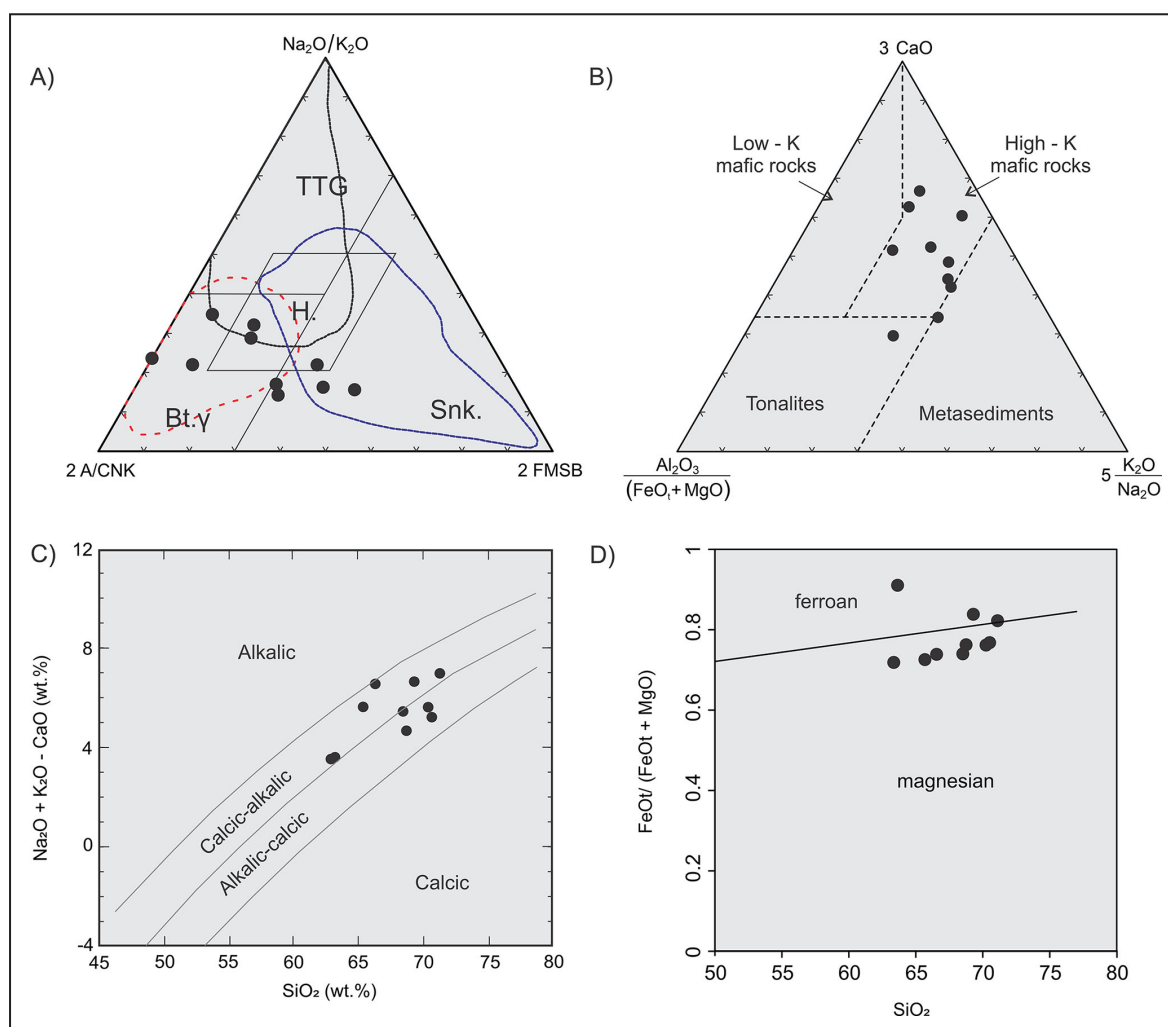


**FIGURE 7.** (Binary and ternary diagrams showing composition in terms of major elements in the granodioritic to tonalitic orthogneisses of the Granjeiro Complex. (A) Ternary classification diagram from Laurent et al. (2014) for the case of late Archean granitoids:  $\text{Na}_2\text{O}/\text{K}_2\text{O}$  vs.  $2^*\text{A/CNK}$  vs.  $2^*\text{FMSB}$ . Subtitle: Snk. – Sanukitoid; Bt.  $\gamma$  = biotite bearing granite; H. = hybrid rocks; (B) Ternary diagram  $\text{Al}_2\text{O}_3/(\text{FeO} + \text{MgO})$  vs.  $3\text{CaO}$  vs.  $5(\text{Na}_2\text{O}/\text{K}_2\text{O})$  by Laurent et al. (2014). The fields represent the composition of magmas derived from potential sources; (C) Diagram  $\text{Na}_2\text{O} + \text{K}_2\text{O} - \text{CaO}$  (wt. %) vs.  $\text{SiO}_2$  by Frost et al. (2001); (D) Binary diagram  $\text{FeOt}/(\text{FeOt} + \text{MgO})$  vs.  $\text{SiO}_2$  (Frost et al. 2001).

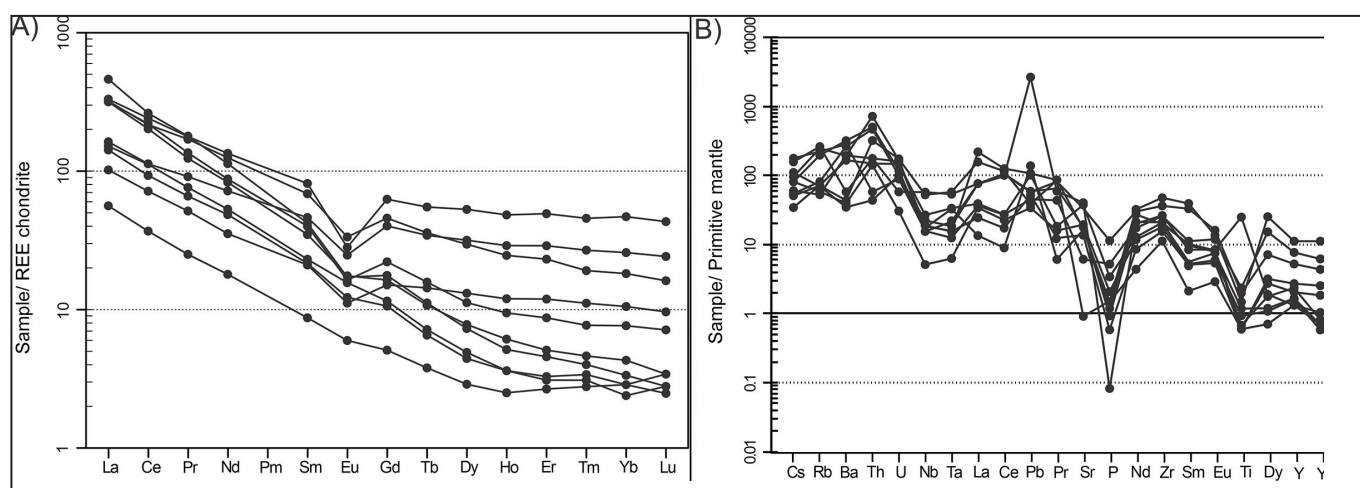


**FIGURE 8.** Geochemistry of trace elements, including rare earth elements for the granodiorite and tonalitic orthogneisses of the Granjeiro Complex: (A) Multi-element diagram for rare earth elements normalized to chondrite (Boynton 1984); (B) Multi-element diagram for trace elements normalized to the primitive mantle (McDonough and Sun 1995).



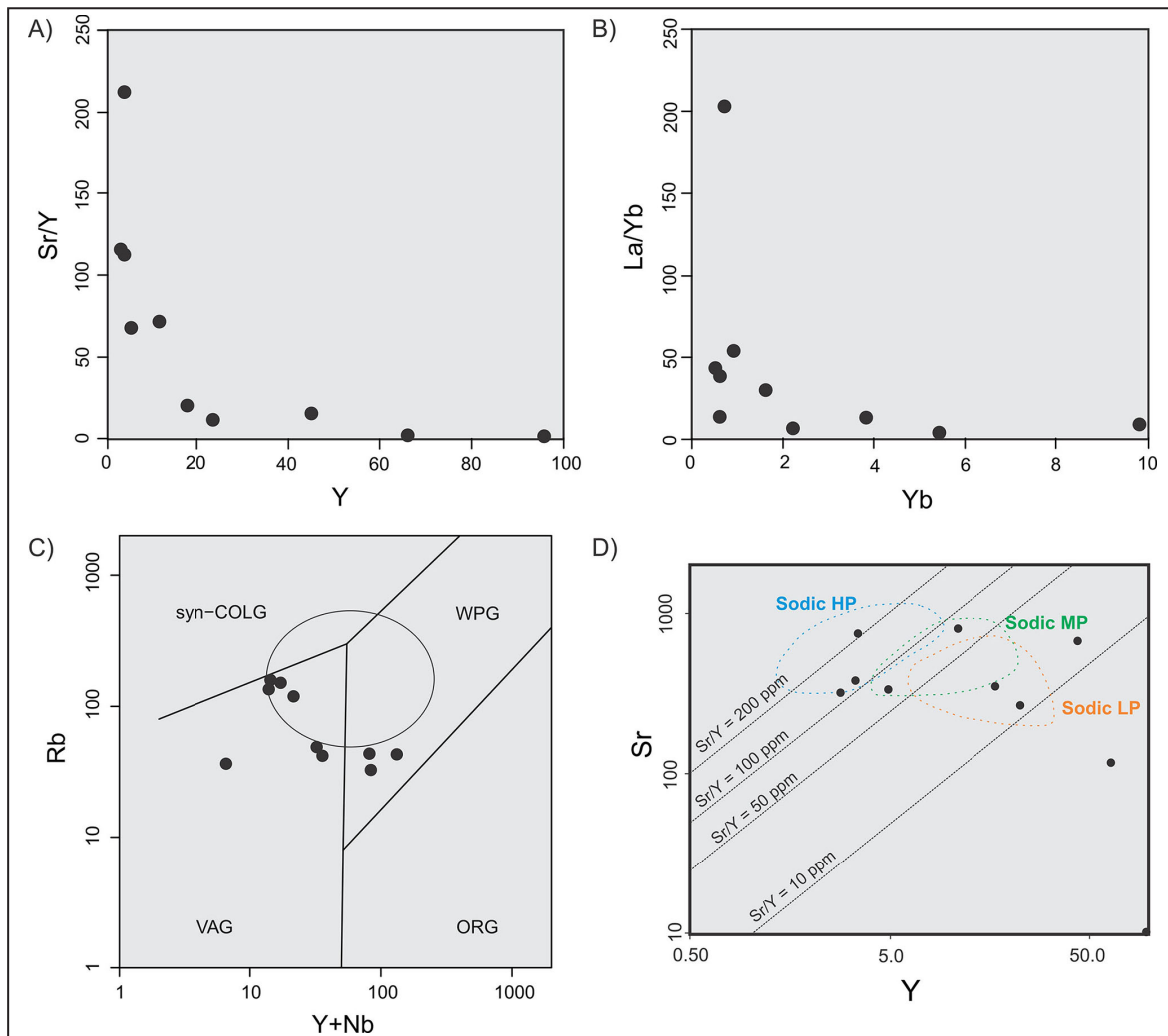


**FIGURE 9.** Discriminant tectonic diagrams for the granodirite to tonalitic orthogneisses of the Granjeiro Complex: (A) Diagram Y vs. Sr/Y by Moyen (2011); (B) Binary diagram Yb vs. La/Yb; (C) Y + Nb x Rb from tectonic discrimination of Pearce (1996); (D) Diagram Sr vs. Y by Moyen (2011) for magma generation conditions in HP (high pressure), MP (medium pressure) and LP (low pressure).

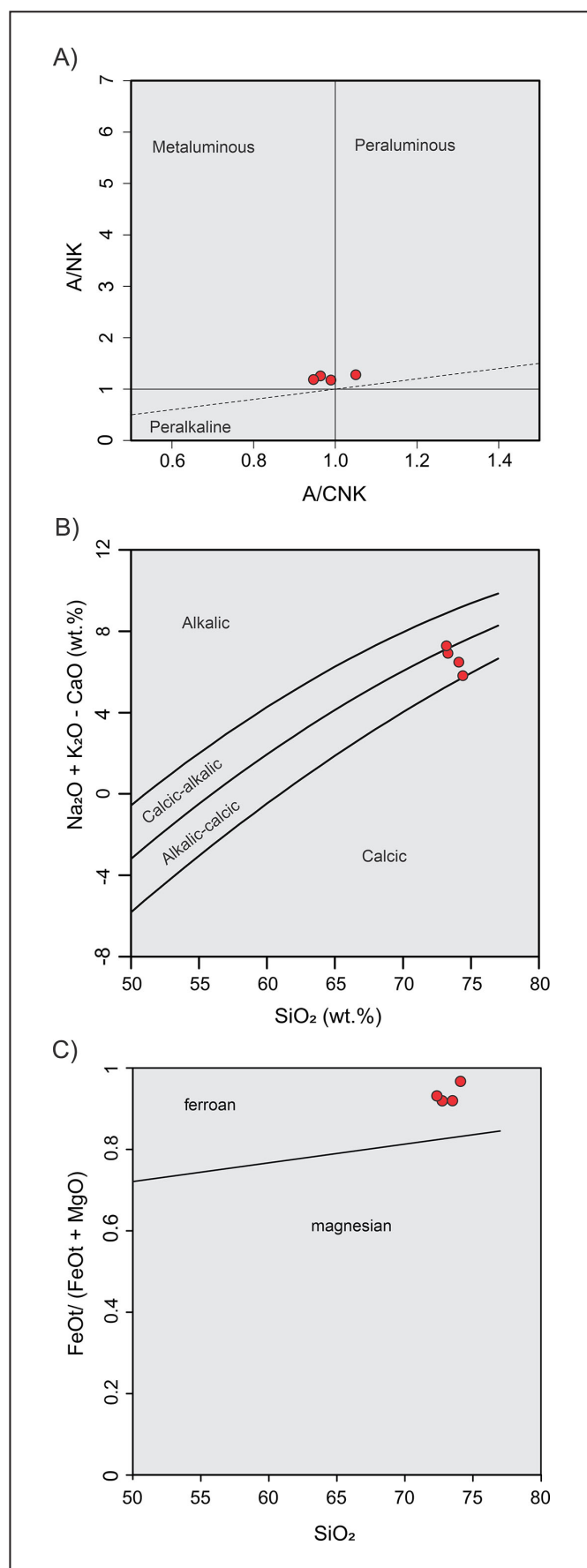
0.76 and 5.4 and reveals an incipient enrichment of ETRL compared to ETRP. When normalized to chondrite (Boynnton 1984), the gneisses exhibit a positive Ce anomaly in some samples (Fig. 11A). In the multielement diagram for trace elements normalized to the primitive mantle of McDonough and Sun (1995), such samples show enrichment in Rb, Th, Ta, Nb, Nd, Y and Yb, indicative of high contents of large-ion lithophile elements and of high force field, in addition to strong Ti depletion, while the Sr and P elements approach the unitary line (Fig. 11B).

Diagram Zr vs.  $10000 \times \text{Ga}/\text{Al}$  by Whalen et al. (1987) used to characterize the origin of the magmatic source of igneous protoliths (Fig. 12A) demonstrates that all samples of syenogranitic orthogneisses are located in the field of type A granites. Likewise, using the Y - Nb - Ce diagram of Eby (1992), they are located in the field of  $A_2$  type granites (Fig. 12B), and the high Y/Nb ratio of the samples indicates generation by partial melting of pre-existing crust. This is corroborated by the binary diagram Rb vs. (Y + Nb) tectonic discrimination of Pearce (1996), whose samples plot in the intraplate field and coincide with the field of post-collisional intraplate granites (Fig. 12C).

### 6.3. Metamafic rocks

The seventeen samples of mafic metavolcanic rocks from the Granjeiro Complex have high  $\text{Al}_2\text{O}_3$  contents (10 to 17%) and  $\text{Fe}_2\text{O}_3$  (7 to 16%), average  $\text{SiO}_2$  concentrations (46 to 55%) and MgO (6 to 11%) at low contents of CaO, MnO,  $\text{TiO}_2$ ,  $\text{Na}_2\text{O}/\text{K}_2\text{O}$  and  $\text{P}_2\text{O}_5$  (Appendix 3). In AFM diagram of Irvine and Baragar (1971), in diagram Nb/Y vs.  $\text{Zr}/\text{P}_2\text{O}_5$  (Floyd and Winchester 1975) and in the Jensen diagram (1976), the metamafic rocks of the Granjeiro Complex demonstrate affinity with high Fe tholeiitic basalts (Fig. 13).

Metamafic rocks have  $\Sigma\text{ETR}$  values between 23 and 107 ppm.  $\text{Eu}/\text{Eu}^*$  ratio values are non-existent in most samples, however slightly positive or negative values are present in some rocks. The pattern of metamafic rocks in the ratio  $(\text{La}/\text{Yb})_N$  shows incipient to high enrichment of heavy rare earth elements when compared to light rare earth elements, with values between 1.27 and 6.75. When normalized to chondrite (Boynnton 1984), metamafic samples show negative Ce anomalies (Fig. 14A), reflecting the general behavior of a volcano-exhalative environment. For the analysis of trace elements, normalized to the primitive mantle (McDonough



**FIGURE 10.** Classification diagrams of the syenogranitic gneisses belonging to the Granjeiro Complex: (A) A/CNK – A/NK diagram from Shand (1943); (B) Diagram (Na<sub>2</sub>O+K<sub>2</sub>O – CaO) wt. % vs. SiO<sub>2</sub> by Frost et al. (2001); (C) diagram FeOt/(FeOt + MgO) vs. SiO<sub>2</sub> (Frost et al. 2001).

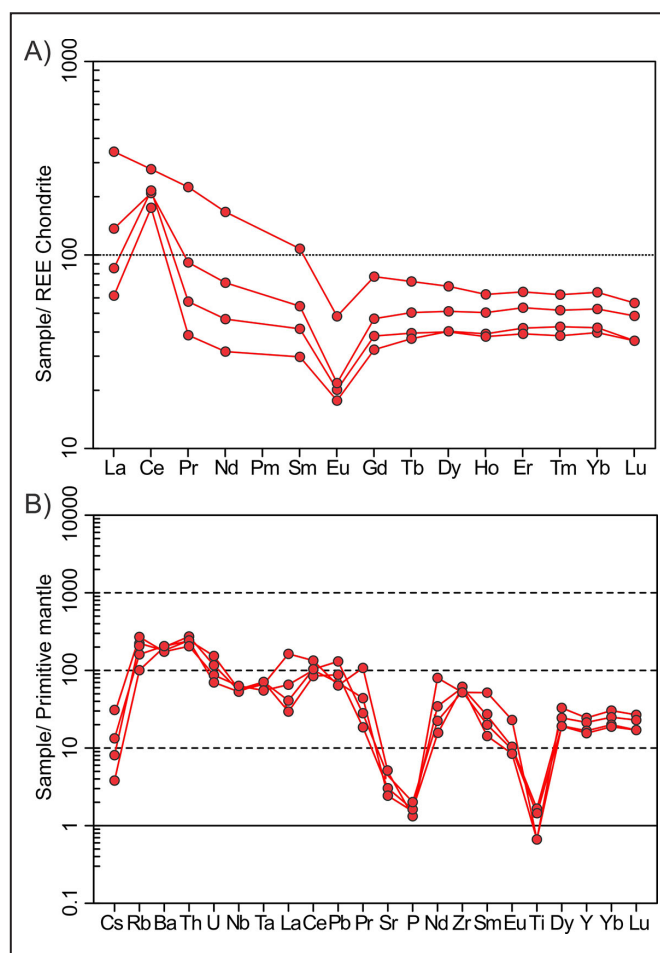


**FIGURE 11.** Multielement diagrams of syenogranitic orthogneisses: (A) Rare earth elements normalized to chondrite (Boynton 1984) and (B) Trace elements normalized to early mantle (McDonough and Sun 1995).

and Sun 1995), metamafic samples are enriched in lithophile elements and enriched in high field force elements, mainly Pb, Th and U (Fig. 14B), however, many samples also present negative Ta values.

In the tectonic discrimination diagrams of Pearce et al. (1977) and Mullen (1983) metamafic samples have a composition similar to island arc tholeiites (Fig. 15).

#### 6.4. Metaultramafic rocks

The six samples of ultramafic metavolcanic rocks from the Granjeiro Complex have high concentrations of MgO (18 to 20%) and Fe<sub>2</sub>O<sub>3</sub> (9 to 15%), medium Al<sub>2</sub>O<sub>3</sub> content (4.5 to 7.5%) and SiO<sub>2</sub> (44 to 51%) and low concentrations of CaO, MnO, TiO<sub>2</sub>, N<sub>2</sub>O/K<sub>2</sub>O and P<sub>2</sub>O<sub>5</sub> (Appendix 4). In AFM diagram of Irvine and Baragar (1971), in diagram Nb/Y vs. Zr/P<sub>2</sub>O<sub>5</sub> (Floyd and Winchester 1975) and in the Jensen diagram (1976), the ultramafic rocks show a transitional composition from komatiite basalt to komatiite (Fig. 13).

Metaultramafic rocks have ΣETR values between 36 and 94 ppm. Eu/Eu\* values indicate strong negative Eu anomalies, whose values are between 0.57 and 0.83, while the ratio (La/Yb)<sub>N</sub> varies between 3.63 and 6.04 and reveals greater enrichment in heavy rare earth elements when compared to light rare earth elements. When normalized to chondrite

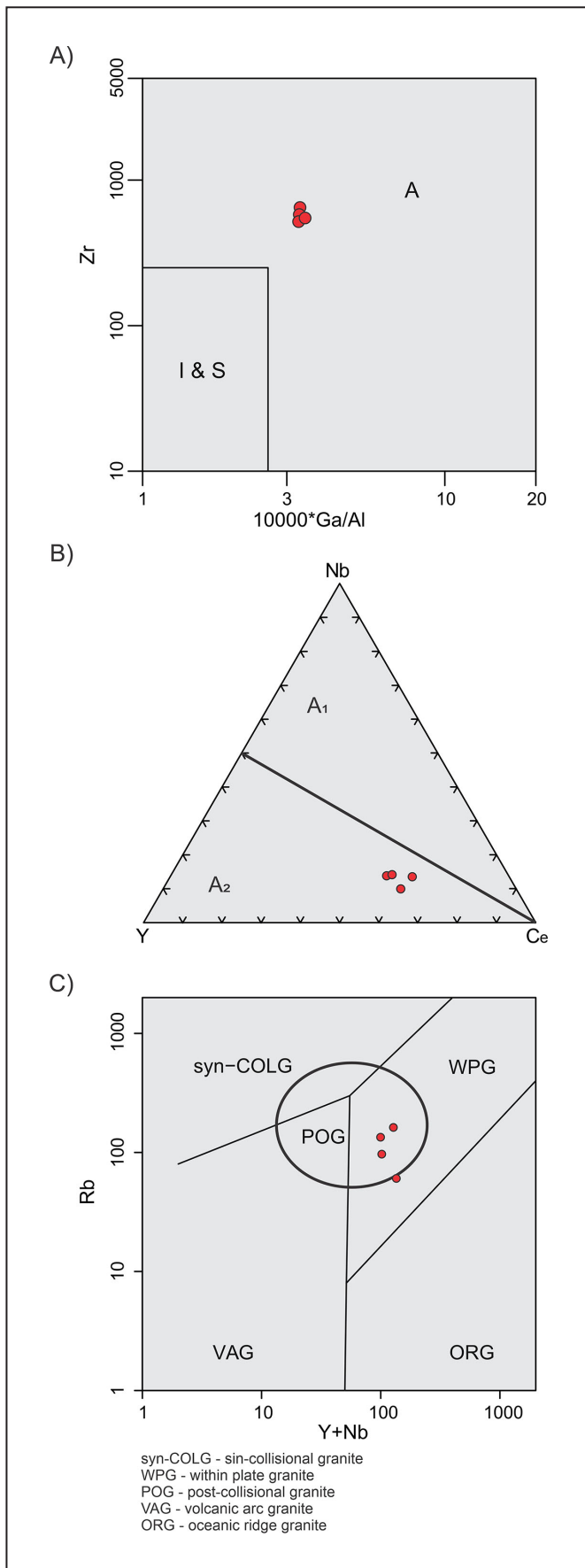


**FIGURE 12.** Discriminant tectonic diagrams of syenogranitic orthogneisses. (A) Diagram Zr vs.  $10000 \cdot \text{Ga}/\text{Al}$  (Whalen et al. 1987); (B) ternary diagram Y-Nb-Ce (Eby 1992); (C) diagram Rb-(Y + Nb) (Pearce 1996).

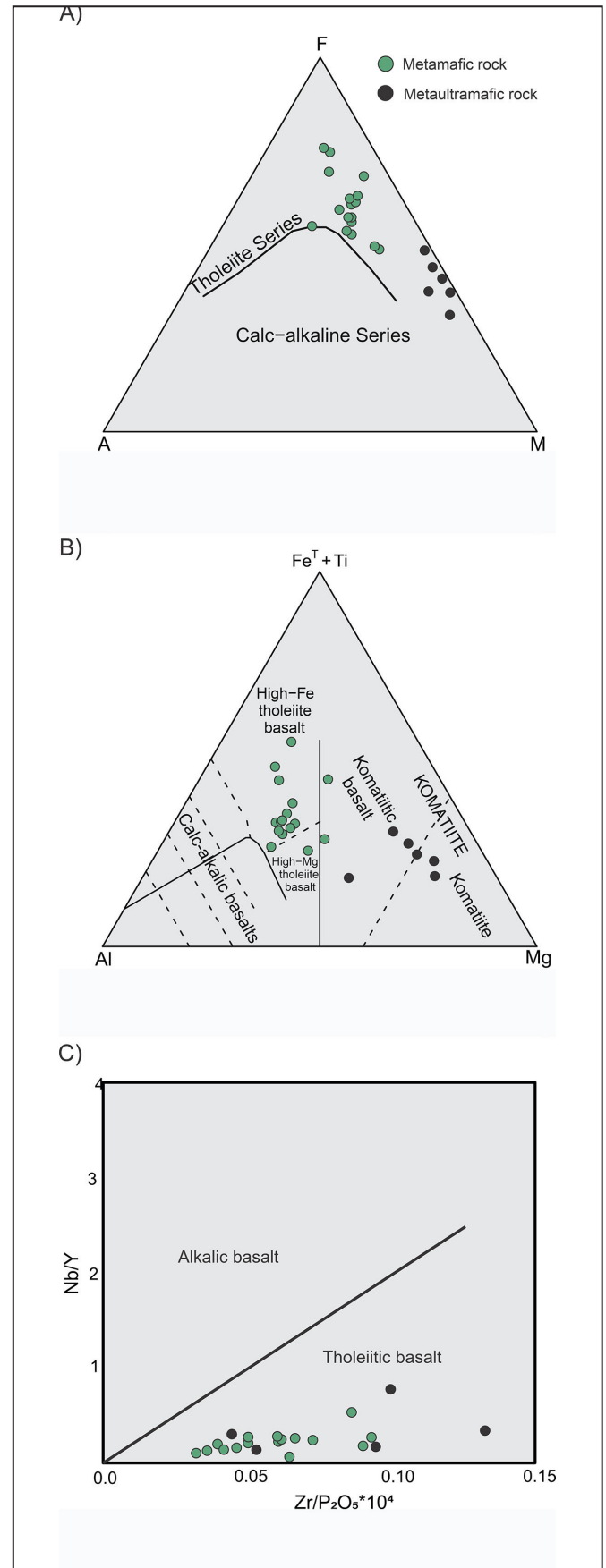


**FIGURE 13.** Classification diagrams for the metamafic and metaultramafic rocks of the Granjeiro Complex. (A) Diagram AFM by Irvine and Baragar (1971); (B) Diagram Nb/Y vs.  $\text{Zr}/\text{P}_2\text{O}_5$  (Floyd and Winchester 1975); (C) Ternary diagram Al vs.  $\text{Fe}^T + \text{Ti}$  vs. Mg (Jensen 1976).



(Boynton 1984), similar to samples of the metamafic lithotype, the metaultramafic samples present negative Ce anomalies (Fig. 14C), while in the multi-element diagram of trace elements normalized to the primitive mantle (McDonough and Sun 1995) such samples show strong depletion in lithophile elements (K, Rb, Cs, Sr and Ba) and significant enrichment in the group of high-field elements of force (Fig. 14D).

In the tectonic discrimination diagrams of Pearce et al. (1977) and Mullen (1983) the samples present a well defined trend (Fig. 15). Metaultramafic rocks have a composition similar to boninites and transition to generation in environments analogous to island arcs, represented by metamafic rocks.

### 6.5. Banded iron rocks (RFB)

Sixteen representative samples of RFBs have  $\text{SiO}_2$  content in the range of 37 to 50% and  $\text{Fe}_2\text{O}_3$  values between 41 and 67%, while the other larger elements have a low percentage. The contents of MgO (up to 2.5%) and CaO (2.2%) are higher when the RFBs have amphibole in their composition (Appendix 5). The  $\Sigma\text{ETR}$  values vary from 10 to 100 ppm. The ratio  $(\text{La}/\text{Yb})_N$  varies from 0.6 to 2.7, indicating insignificant enrichment of light rare earth elements in some samples that present a

predominant flat pattern.  $\text{Eu}/\text{Eu}^*$  ratio values indicate a weak positive anomaly between 1.0 and 1.14, however, negative Ce anomalies can be observed.

In trace element diagrams normalized to the early mantle (McDonough and Sun 1995) and PAAS (Post Archean Australian Shale; Taylor and McLennan 1985), (Fig. 16A), the samples show enrichment in lithophile elements, such as Cs, Ba, U, Pb, La and Y (with the exception of Sr), with strong negative anomalies also being observed in high field strength elements (Th, Nb, Ta, Zr and Ti). Figure 16B reflects the marked depletion of trace elements by at least one magnitude over the PAAS standard. Elements such as Rb, Ba and La show greater variation in concentration between samples, however, always lower than the standard PAAS unit concentration.

### 7. U-Pb geochronology in zircon

The U-Pb zircon geochronological studies were carried out in four samples from the Granjeiro Complex and associated units, being a migmatitic orthogneiss (sample CB-03), a syenitic orthogneiss (sample JR-333), an amphibolite (sample DJ-07) and a pegmatite granite (JS-289A), whose data are presented

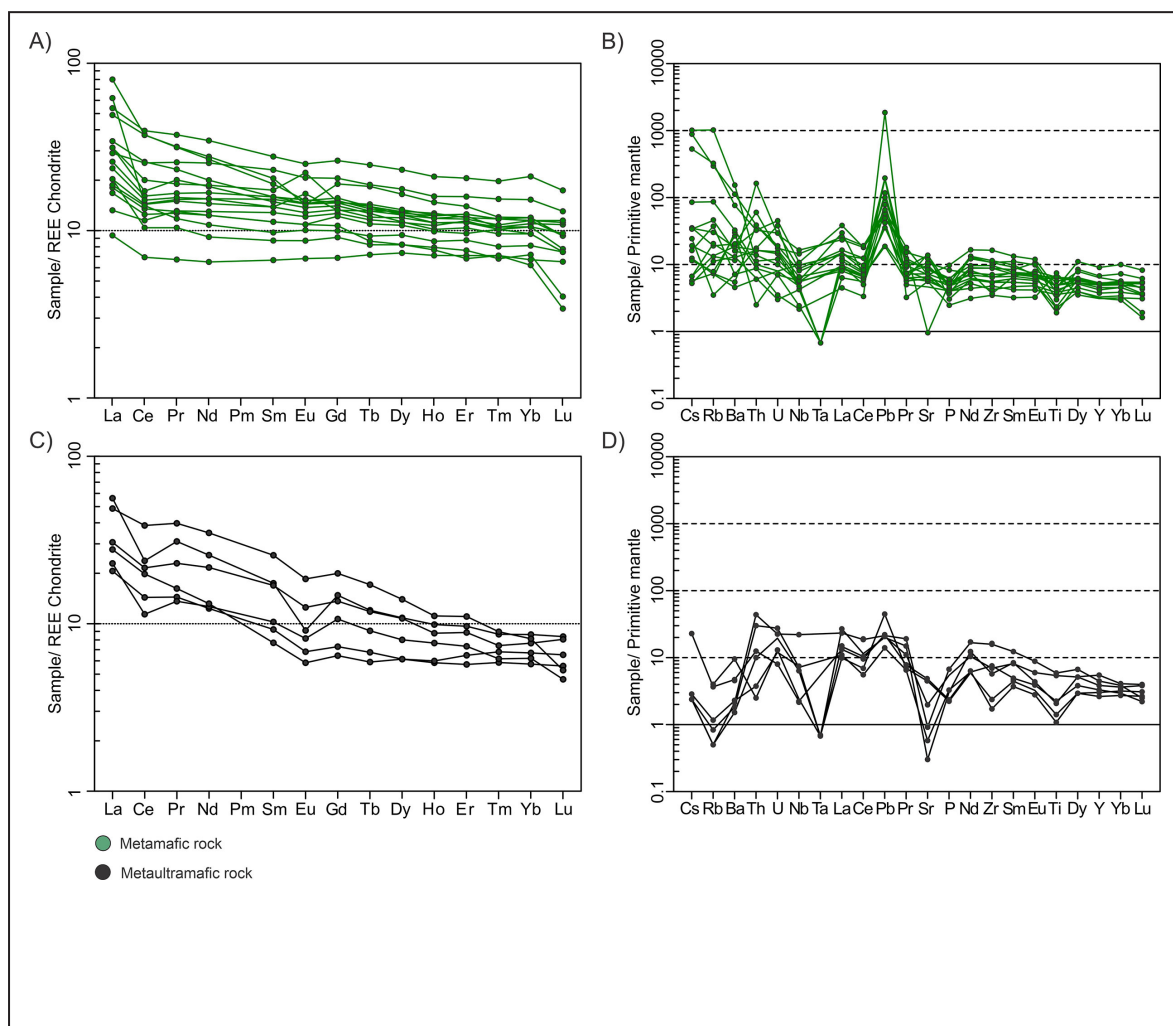


**FIGURE 14.** Multi-element diagrams for the metamafic and metaultramafic rocks of the Granjeiro Complex: (A) Rare earth elements from metamafic samples normalized to chondrite (Boynton 1984); (B) Trace elements for metamafic rocks normalized to the early mantle (McDonough and Sun 1995); (C) Rare earth elements from metaultramafic samples normalized to chondrite (Boynton 1984); (D) Trace elements for metaultramafic rocks normalized to the early mantle (McDonough and Sun 1995).

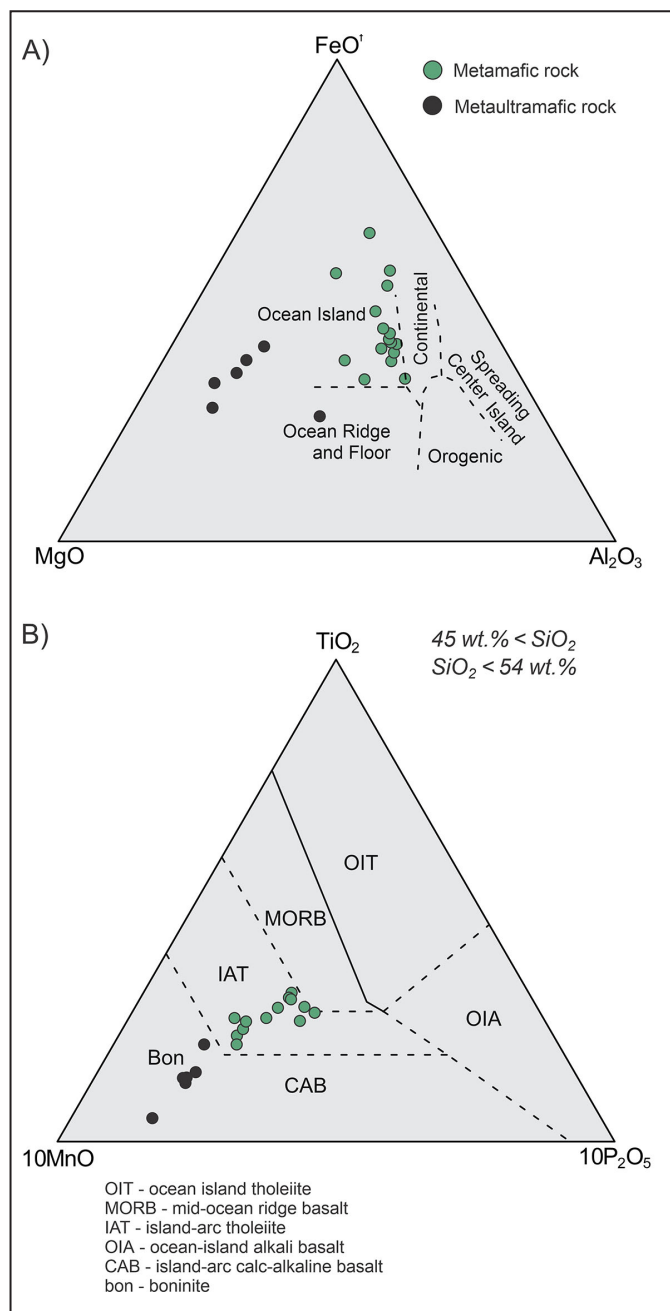


FIGURE 15. Tectonic discrimination diagrams for the metamafic and metaultramafic rocks of the Granjeiro Complex: (A) Diagram by Pearce et al. (1977); and (B) Mullen diagram (1983).

in Appendices 6 to 9. Cathodoluminescence images of zircon crystals and concordia diagrams are shown in Fig. 17.

### 7.1. Migmatitic orthogneiss (Leucosome)

Sample CB-03 refers to an outcrop of migmatite orthogneiss composed of tonalitic mesosome and leucosome of granitic composition. Priority was given to dating the leucosome in order to define the age of metamorphism. The zircon grains obtained, in general, are well formed, euhedral and subhedral, angular to subangular and with dimensions between 110 and 250  $\mu\text{m}$ , with some crystals having metamorphic zoning, shown in Figure 17A related to metamorphic events. Isotopic analysis of the zircon grains (Appendix 6) resulted in two discordant ages (Fig 17A) with an upper intercept calculated as nine spots of  $3349 \pm 15$

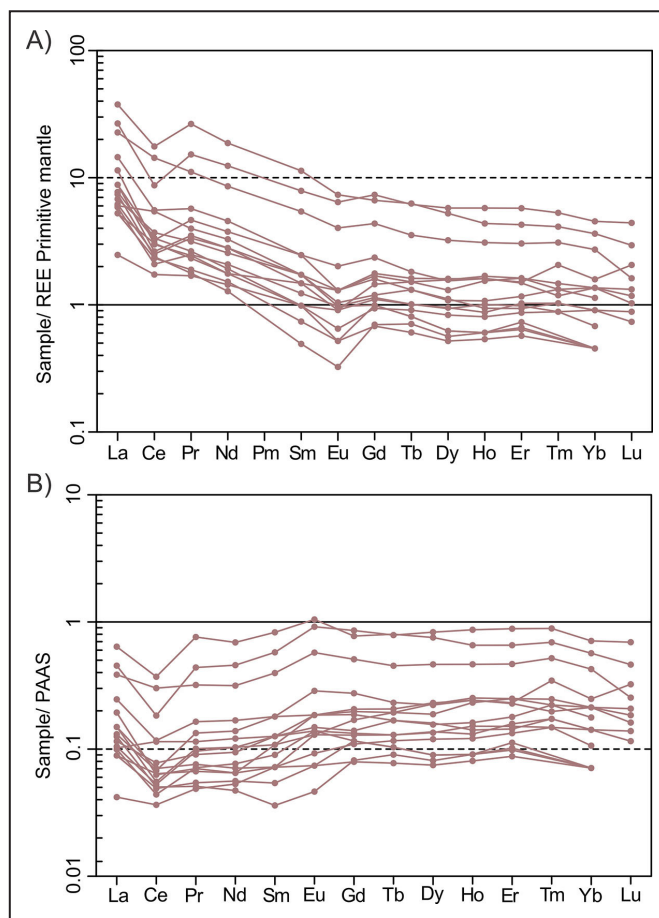


FIGURE 16. (A) Multi-element diagram for trace elements in banded iron rocks normalized to the early mantle (McDonough and Sun 1995); (B) Trace elements in banded iron rocks normalized to PAAS (Taylor and McLennan 1985).

Ma (MSWD = 0.62), interpreted as the age of crystallization of the tonalitic protolith, and the second intercept defined by a small amount of four spots presented a value of  $1941 \pm 27$  Ma (MSWD = 1.04), representing a metamorphic event responsible for anatexis and formation of the leucosome.

### 7.2. Syenogranitic orthogneiss

Sample JR-333 represents a mylonitic syenogranitic orthogneiss and presented few zircon grains (Appendix 7), many fractured, generally with corroded edges and subhedral and anhedral shapes, with dimensions between 80 and 140  $\mu\text{m}$ . The U/Th ratio varies from 0.09 to 1.28, suggesting a probable igneous origin. The age obtained defined a value of seven spots of  $2628 \pm 8$  Ma (MSWD = 4.87), interpreted as the crystallization age of the protolith (Fig. 17B).

### 7.3. Amphibolite – Metavolcanosedimentary unit

The selected amphibolite corresponds to sample DS-07 (Appendix 8) whose zircon grains are clear and sub-rounded, with sizes varying between 70 and 220  $\mu\text{m}$ . The morphology of these zircons is associated with crystallization at high temperatures, which allows the age obtained to be interpreted as associated with the metamorphic peak undergone by the rock. Thus, in the Concordia diagram, the analyzed zircons defined a concordant age of 20 spots at  $2200 \pm 4$  Ma

(MSWD = 0.22), interpreted as the age of metamorphism and deformation of the sample (Fig. 17C).

#### 7.4. Pegmatitic granite body

Sample JR-289A represents an intrusive granitic body in the orthogneisses. Zircon grains (Appendix 9), in general, have subhedral or anhedral prismatic shapes, dimensions that vary between 90 and 220  $\mu\text{m}$ , are metamictized, have corroded edges and may present zoning. The results of the analysis showed great variation in age values (Fig.17D). One set of zircon grains showed an older concordian age of 2651

$\pm 9$  Ma (MSWD = 1.5). Two other age intervals indicated  $2163 \pm 8$  Ma (MSWD = 2.9) and  $2106 \pm 12$  Ma (MSWD = 0.01). The youngest concordia had an age of  $1759 \pm 34$  Ma (MSWD = 5.2), defined as the age of crystallization of the body.

#### 8. Sulfur isotopes in pyrite

Four pyrite samples from amphibolites were analyzed (Table 1). Pyrite is late generation as it is present in fracture systems that cut the host rocks.

The values of  $\delta^{34}\text{S}$  range from -3.11 to +2.03‰. The small isotopic variation may be indicative of a single sulfur source.

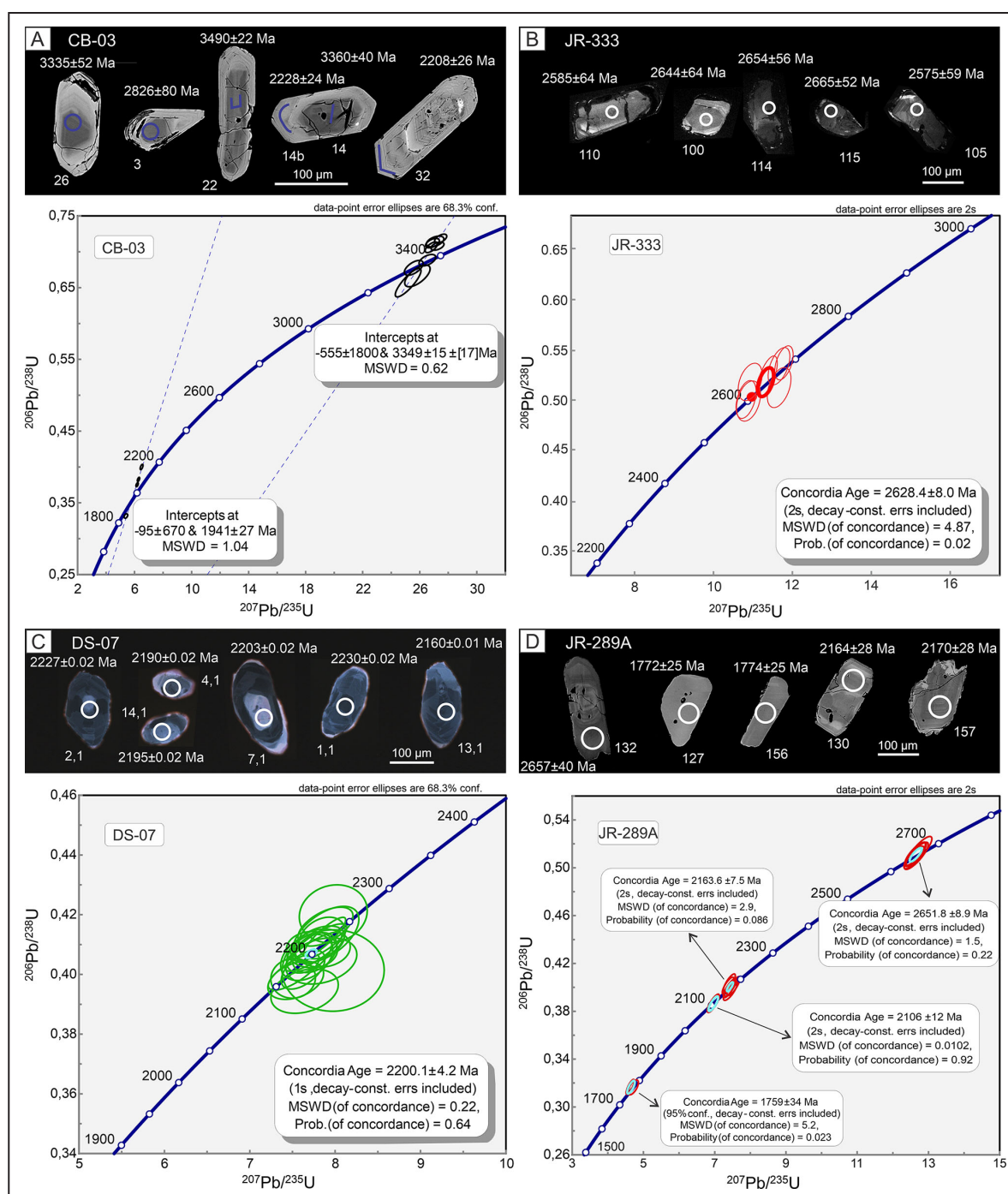


**FIGURE 17.** Cathodoluminescence images of zircon grains and age diagrams of: (A) Migmatitic orthogneiss (sample CB-03); (B) Syenogranitic orthogneiss (sample JR-333); (C) Amphibolite (sample DS-07); and (D) Pegmatitic granite body (sample JR-289A).



According to Ohmoto and Rye (1979), values of  $\delta^{34}\text{S}$  close to zero are consistent with a single sulfur source. Chaussidon and Lorand (1990) assign to mantle sources values of  $\delta^{34}\text{S} = 0 \pm 3\text{‰}$ . Therefore, the results obtained in the pyrite samples converge to a magmatic source, which may be related to the exsolution of magmatic fluids containing sulfur from igneous intrusion or even leaching of sulfur from magmatic rocks during the fluid-rock interaction process.

**TABLE 1** – Isotopic composition ( $\delta^{34}\text{S}$  ‰, V-CDT) of sulfur isotopes of pyrite crystals from amphibolite samples from the Granjeiro Complex.

Sample	$\delta^{34}\text{S}$ ‰ V-CDT
JR-334	-2.32
JR-343	+2.03
JR-345A	+1.34
JR-345D	-3.11

## 9. Discussions

### 9.1. Tectono-magmatic characterization of the Granjeiro Complex

The protoliths of the Granjeiro Complex orthogneisses are represented by magmatic rocks with significant variation in silica content and high values of  $\text{Na}_2\text{O}$  and  $\text{Al}_2\text{O}_3$ . This characteristic is reflected in the chemical classification of these rocks, which present tonalitic to granodioritic compositional variation, magnesian geochemistry that can transition to ferrous types and alkalic-calcic to calcic composition. Previous studies by Vasconcelos and Gomes (1998) in the Granjeiro – Ceará region indicated calcium-alkaline affinity of these rocks, as well as mantle derivation and generation in magmatic arc configuration.

The multi-element diagram shows low LILE and HFSE element contents. The low concentration of Nb and Ta points to characteristics of rocks crystallized in a magmatic arc environment, being evident not only in the rocks under discussion, but also in other lithotypes of the Granjeiro Complex. Typically, the values of the elements Sr, Y and Yb in orthogneisses, which are relatively immobile and sensitive to temperature and pressure variations in the melting of the parent rock, indicate petrogenetic origin in environments of different pressures, probably associated with the melting of metabasalt at different depths. (Moyen and Stevens 2006; Moyen 2011; Moyen and Martin 2012; Laurent et al. 2014).

The orthogneisses studied can be considered more evolved, within the diachronic framework of Archean rocks of TTG suites, representing greater fractionations of ETRL compared to ETRP in the analysis of ETR normalized to chondrite, in addition to significant, negative or positive Eu anomalies. These features are also interpreted as indicative of magma generation sources at low (negative Eu) or high pressure (positive Eu), with melting at different levels in the plagioclase stability field. The enrichment in incompatible elements such as Th, Pb, U, Cs and Rb may be linked to the process of partial melting of the metasomatized mantle, as well as due to the evidence of potassium hydrothermal alteration that is recognized in these rocks.

As previously mentioned, the orthogneisses of the Granjeiro Complex can be correlated to the melting of K-rich mafic magmas originating from metasomatized mantle, with

a possible subordinate contribution from younger generations of melting of pre-existing TTG rocks in the primitive crust. TTG rock suites are the main products of crustal accretion processes during the Archean, whose continents are generally formed by subduction of oceanic plates (Martin 1994, Foley et al. 2002; Rapp et al. 2003) or in settings similar to modern plate tectonics, which includes oceanic plateaus (Smithies and Champion 2000; Bédard 2006; Willbold et al. 2009). According to the literature, these rocks formed more than 50% of the volume of the continental crust generated during the Archean Eon (Armstrong 1981; Taylor and McLennan 1985, 1995; Belousova et al. 2010; Dhuime et al. 2012) and have unique geological characteristics, in terms of petrographic, chemical and petrological attributes (Condie 1981; Taylor and McLennan 1985; Martin 1994; Percival 1994; Keller and Schoene 2012), reflecting a fundamental period of geodynamic change on the planet (Windley 1984; Taylor and McLennan 1995; Condie and O'Neill 2010).

Considering the U-Pb age in zircon of 3.35 Ga Ma obtained in the leucosome of the migmatite orthogneiss of the Granjeiro Complex (sample CB-03), this is interpreted as-of crystallization of the igneous protolith of gneiss in the Paleoproterozoic. This age is consistent with data presented by Martins (2017) of 3.42 Ga, Pitarello et al. (2019) of 3.51 Ga and Brito Neves et al. (2022) of 3.58 Ga for the Granjeiro Complex rocks. However, these ages in the range of 3.5 to 3.3 Ga are outside what was defined by Laurent et al. (2014) for the period from 3.0 to 2.5 Ga as the most important for the generation of TTG granitoids, which demonstrates the importance of the Paleoproterozoic rocks of the Granjeiro Complex for the reconstruction of crustal evolution processes during the Paleoproterozoic and its long-term evolutionary model (Friend and Nutman 2005; Zhai et al. 2006; Moyen and Stevens 2006; Moyen 2011; Moyen and Martin 2012; Laurent et al. 2014).

However, previous studies in the Granjeiro Complex in the Granjeiro region – Ceará, such as those by Bautista (2012), Freimann (2014), Pitarello et al. (2019) and Gomes et al. (2021) provided U-Pb dating data for orthogneisses that fall in the 3.10 to 3.0 Ga interval. This information suggests that the protocrust, composed of Paleoproterozoic protoliths from the Granjeiro Complex, experienced juvenile crustal accretion during the Mesoarchean. This demonstrates that the process of crustal evolution in the Complex was continuous throughout the entire Archean Eon.

The metavolcanosedimentary unit of the Granjeiro Complex is composed of metamafic rocks (amphibolites and metagabbros), metaultramafic rocks (magnesian schists and serpentinites), quartzites and banded iron rocks. These lithotypes are usually intercalated and represent subverticalized bodies transposed by Neoproterozoic NE to E-W shear zones. Amphibolites derive from tholeiitic basalts and have a chemical composition analogous to that of modern island arcs, related to the initial development of subduction zones between oceanic plates, with partial melting of the subducted plate. Previous lithochemical studies by Santos et al. (2014), near the municipality of Curral Novo do Piauí - Piauí, and Ancelmi (2016) near the municipality of Granjeiro - Ceará, describe this association as generated in a back-arc basin through a subduction system.

Metaultramafic rocks have komatiitic affinity with boninitic similarity (Mullen 1983) generated through subduction involving two oceanic plates in a low degree of partial melting

in the deep mantle, such as the subducted lithosphere or the Archean mantle (Kearey et al. 2009). Tectonic environment discriminant diagrams demonstrate a *trends* evolutionary process during the generation of mafic/ultramafic magmatism. Previously, Pitarello et al. (2019) noted the similarity of the metaultramafic rocks of the Granjeiro Complex with boninites or komatiites, whose trace element content corroborates this affinity. Metaultramafic rocks are depleted in LILE elements, while metamafic rocks have high LILE content, such as Sr, Ba, Cs, Rb and Ti (Gill 2010). The behavior of Ti tends to vary depending on pressure during magma generation. In calcium-alkaline ultramafic magmas generated during the initial phase of subduction at high pressure and low degree of partial melting, premature saturation of plagioclase occurs. Furthermore, the fractionation of Al, Ti and Fe is controlled by the crystallization of olivine and clinopyroxene, resulting in greater depletion of these elements in solidified rocks (Best 2003). In contrast, metamafic rocks formed in island arcs were generated in low-pressure environments where plagioclase fractionation occurs before pyroxene in the magma. In this way, plagioclase rejects the elements Fe and Ti, resulting in a *trends* enrichment in these elements (Albarède 2009). The ETR data normalized to the chondrite of the studied samples indicate that there is a slight fractionation of ETRP in relation to ETRL (Fig. 14a), which configures an arc environment characteristic. The Eu/Eu\* ratio indicates a strong negative Eu anomaly, together with Ce, for ultramafic rocks, which exhibit a more primitive character than mafic rocks and crystallization conditions associated with oxidizing environments.

The ages of the intervals attributed to metamafic and metaultramafic rocks in the literature correspond to two distinct intervals: 3.0 Ga (Freimann 2014) and 2.8 to 2.6 Ga (Bautista 2012; Ancelmi 2016; Pitarello et al. 2019; Brito Neves et al. 2022). Freimann's (2014) geochronological information for hornblende was excluded from the regional analysis due to high uncertainty, due to the high MSWD associated with it. As a result, the Neoproterozoic interval is considered the period of formation of the metavolcano-sedimentary association. Ancelmi (2016), when studying the metamafic and metaultramafic rocks in the Arrojado – Ceará region, developed a tectonic model that suggests that the metavolcano-sedimentary sequence represents a *greenstone belt* formed in a basin of back arc which developed in a subduction system, with the generation of a continental magmatic arc around ca. 2.7-2.6 Ga.

The banded iron rocks present a mineral association consistent with the sedimentary facies described by Pitarello et al. (2019). The RFBs are predominantly derived from the oxide facies, with a predominant constitution of quartz and magnetite. The presence of grunerite indicates a transition to the silicate facies or metamorphic stabilization of the two precursor minerals (quartz and magnetite). Although the microstructure information from the RFBs shows superposition of the tectonic activity of the Brazilian event, influenced by transcurrent shear zones with a high angle of NE-SW direction, previous stages of metasomatism can still be identified, such as the presence of quartz and carbonate veins, generation of hydrothermal magnetite and martitization. The analysis of trace elements normalized to the primitive mantle shows that the RFB samples are strongly depleted in HFSE elements, a factor indicative of the absence of clastic contribution in the depositional environment (Bau and Moeller

1993; Bolhar et al. 2004; Pecoits et al. 2009; Basta et al. 2011). Santos et al. (2014) identified two types of iron rocks in the area of the Curral Novo iron district: the first is of the Algoma type, originating from chemical precipitation and associated with metagabbros and metabasalts that underwent metamorphism in the amphibolite facies and the second is tectonocontrolled and occurs in a disseminated, irregular, laminated and in gaps, consistent with the foliation. ETRs normalized to PAAS indicate, in general, low ETR content, slightly positive Eu anomaly and considerable variation in the fractionation of ETRL over ETRP (Fig. 16b), on average with greater impoverishment of the former. The spectrum of values indicates the prevalence of low-temperature fluids, with precipitation of sediments at a great distance from the fumaroles (Bau and Möller 1993; Bolhar et al. 2004; Alexander et al. 2008). The depletion of ETR in relation to PAAS also allows inferring the low influence of surface waters, revealing precipitation outside continental areas (Elderfield et al. 1990; Alexander et al. 2008). The negative Ce anomaly present in the samples suggests oxidizing conditions in the ocean during iron precipitation (Kato et al. 2002). This oxidizing condition could have occurred before the Great Oxidation Event in restricted oceans (Kato et al. 2006; Frei et al. 2008). Alternatively, negative Ce anomalies may be the result of oxidation due to weathering processes.

## 9.2. Neoproterozoic crustal growth

The U-Pb age in zircon of 2.63 Ga obtained in syenogranitic orthogneiss indicates magmatic activity at the end of the Neoproterozoic whose igneous protolith intruded the Paleoproterozoic rocks and the volcanosedimentary association of the Granjeiro Complex.

Syenogranitic orthogneisses have high alkali and silica contents and low concentrations of other larger elements, present in few mafic minerals, such as hornblende and biotite. Its chemical classification includes ferrous and metaluminous composition, transitioning to peraluminous and alkalic-calcic affinity. Chondrite-normalized ETR content in most samples shows a slight enrichment of ETRL over ETRP in a gull-like pattern (Fig. 11a). The strong negative Eu anomaly is associated with the removal of plagioclase in the partial melting of felsic magma, while the enrichment of Ce in the samples indicates reducing crystallization conditions. In the trace element diagram normalized to the primitive mantle (McDonough and Sun 1995), the granites are enriched in Rb, Th, Ta, Nb, Nd, Y and Yb, indicative of high content of LILE and HFSE elements, as well as strong depletion of K and Ti. These characteristics are very similar to type A granites described in the literature (Whalen et al. 1987; Eby 1992; Grebennikov 2014). The samples under study plotted mostly type A<sub>2</sub> of the diagram of type A granites (Fig. 12b) proposed by Eby (1992). This typology characterizes granitic rocks that occur in post-collisional settings, corroborating a younger Neoproterozoic event. This information adds to the U-Pb geochronology data in the 2.6 to 2.5 Ga interval already available in the literature (Silva 1997; Martins 2017; Pitarello et al. 2019; Gomes et al. 2021; Brito Neves et al. 2022). The representativeness of these data shows that crustal growth during the Neoproterozoic was notable, mainly characterized by the intrusion of type A<sub>2</sub> rocks in the lithotypes of the Granjeiro Complex.



Similar to the metavolcanosedimentary unit, these gneisses also underwent metasomatism, presenting different types of hydrothermal alteration, mainly represented by silicification, albitization and potassium alteration. Carbonatization and sulfide formation occur as late alteration, although these processes do not present pervasive modification as are commonly observed in host rocks.

### 9.3. Intrusion of Paleoproterozoic granite bodies and metasomatism

The intrusion of pegmatite granitic bodies of syenogranitic or syenitic alkali feldspar composition is recognized in most of the lithotypes described in the study area and significantly affects the host rocks through metasomatic processes. The hydrothermal alterations listed include silicification, albitization, carbonatization, potassium alteration, sericitization and the formation of garnet and muscovite, or sulfides. Geochronological dating using the U-Pb method on zircon of these pegmatite granites showed four distinct families of zircon with a wide range of ages. Three concordia ages resulted in values of 2.65 Ga, 2.16 Ga and 2.1 Ga, which were interpreted as zircons inherited by crustal assimilation, with the oldest age being compatible with the crystallization age of syenogranitic orthogneisses. The set of zircons aged 1.76 Ga is interpreted as the crystallization age of these pegmatite granites.

In the literature, dating of orthogneisses with quartz-dioritic and granodioritic compositions were reported by Bautista (2012) and Ancelmi (2016), revealing ages at 2.4 Ga. Ancelmi (2016) suggests that these gneisses are evidence of crustal growth that occurred during the Siderian. Furthermore, Ancelmi (2016) also presents U-Pb dating data from migmatized rocks with granitic composition, which exhibit ages between 2.2 and 2.1 Ga. These rocks are interpreted as the result of reworking that occurred in the Paleoproterozoic, associated with a continental collision event with juvenile rocks from the Archean microcontinent. This information strengthens the correlation with the age of 2.2 Ga obtained in amphibolite from the Granjeiro Complex, which, in turn, represents the metamorphic peak linked to crustal reworking in the Paleoproterozoic.

Additionally, another significant age is derived from sample CB-03 (leucosome), dated at 1.94 Ga. This age is interpreted as the minimum age of the anatexis-related metamorphic event that occurred in the Orosirian.

### 9.4. Crustal evolution of the Granjeiro Complex

The geodynamic evolution of the Granjeiro Complex, based on new data from this work, in addition to data from the literature, began during the Paleoarchean (3.55 to 3.35 Ga), with the generation of high-K mafic magmas originating from a mantle evolved metasomatized, installed in pre-existing Archean crust (Fig. 18a). At this stage, subduction processes occurred with possible episodes of breakage and sinking of oceanic crust plates (Laurent et al. 2014). This process was responsible for the continental accretion phase in the Mesoarchean (3.1 to 3.0 Ga).

Subduction, involving oceanic plateaus, may have favored the development of the volcano-sedimentary succession, with the generation of mafic and ultramafic magmas and deposition

of exhalative chemical sediments (ca. 3.0 to 2.7 Ga). During the Neoarchean (2.7 to 2.6 Ga) a collisional stage recorded in this Archean block developed. The syenogranitic orthogneisses of post-collisional granitic protoliths of type A2 mark the end of this tectonic stage and indicate the formation of a stable microcontinent at the end of the Archean (Fig. 18b), which was later fragmented (Dantas et al. 2004, 2013; Souza et al. 2016).

The Siderian (~2.4 Ga) was marked by crustal accretion with the crystallization of plutons of quartz-dioritic and granodioritic composition, intrusive in the rocks of the Complex. In the Riachian (2.2 to 2.1 Ga), the dates of migmatized rocks by Ancelmi (2016) and the age of 2.2 Ga obtained in amphibolite from the Granjeiro Complex represent the intense crustal reworking in the Paleoproterozoic. This period was marked in the Complex by high-grade metamorphism, raising the temperature to levels that enabled migmatization in the ortho-derived lithotypes of the Complex, a factor that infers a minimum metamorphic degree in the amphibolite facies. Furthermore, there was stabilization of zircon in amphibolites from the metavolcanosedimentary association. These geological events imprinted on the area are part of an event of regional crustal deformation and high metamorphism that played a fundamental role in the consolidation of the supercontinent Columbia, which formed as a result of the tectonic and metamorphic changes that occurred during the Paleoproterozoic.

As an example, this crustal reworking in the Riachiano is recorded in other complexes existing in the Borborema Norte Subprovince (Dantas et al. 2004, 2013; Gomes 2013; Garcia et al. 2014; Calado et al. 2019; Medeiros et al. 2021; Muniz et al. 2022), in other areas of the Province (Neves et al. 2006) and even in the São Francisco Cráton (Teixeira et al. 2017). That said, it is clear that the Archean-Paleoproterozoic evolution of the Granjeiro Complex coincides with other Archean nuclei in the Borborema North Province, such as the São José do Campestre Massif (Dantas et al. 2004, 2013; Souza et al. 2016), Campo Grande Complex (Ferreira et al. 2020) and Cruzeta Complex (Fetter 1999; Ganade et al. 2017). There is evidence that these complexes were formed from a protocrust derived from the mantle, with the generation of juvenile rocks through accretion in magmatic arc environments and that they were probably fragmented at the end of the Archean to the beginning of the Paleoproterozoic. The ages recorded in these Paleoproterozoic cores in the Borborema Province also coincide with the main magmatic events that occurred during the Archean period in other world provinces (Zhao et al. 2002; Bleeker 2003; Cawood et al. 2013; Condie and Kroner 2013).

The global process of extension of continental masses during the Statherian period (Fig. 18c), after intense metamorphism, crustal reworking and consolidation of the Riachian-Orosirian supercontinent as discussed by Brito Neves et al. (1995), is printed in Complexo Granjeiro. Pegmatite granitic bodies from ca. 1.75 Ga, were responsible for metasomatic processes (sodium alteration with albite, potassium alteration, carbonatization, silicification, reconcentration and enrichment of iron in iron rocks and formation of sulfides). Spatial relationships suggest the installation of a magmatic-hydrothermal system with emanation of magmatic fluids, with fluid-rock interaction processes contributing to the localized generation of concentrations with a high percentage of iron in banded iron rocks. Furthermore, such magmatism resulting from the extensional event in the Statherian period correlates with the Serra do Deserto and

Poço da Cruz suites of the Borborema Norte subprovince, with crystallization ages between 1.80 and 1.74 Ga, corresponding to anorogenic granite protoliths of the *augen* gneisses (Cavalcante 1999; Sá et al. 2014; Pinéo et al. 2023).

## 10. Conclusions

Surveys of field information and petrographic, lithochemical and geochronological U-Pb data in rocks from the Granjeiro Complex and associated units in the Curral Novo do Piauí region indicate that:

- 1 – The Granjeiro Complex consists of a plutono-metavolcanosedimentary association of Paleoproterozoic age intruded by bodies of Neoproterozoic to Statherian age;
- 2 – The granodioritic and tonalitic orthogneisses of the

Granjeiro Complex have significant chemical variation, with a classification corresponding to sanukitoid rocks and granites to biotite, the latter being more evolved. These lithotypes were derived from a high-K mafic metasomatized mantle source, have high ETRL content and high concentration of LILE and HFSE elements. Concentrations in the elements Sr, Y, and Yb and large amplitudes in Eu anomalies (positive and negative) are indicative of magma generation in environments with different pressure sources;

- 3 – The metavolcanosedimentary unit comprises a sequence of metaultramafic, metamafic and banded iron rocks. Metaultramafic rocks have a chemical affinity similar to komatiite basalts. Metamafic rocks have an affinity similar to the chemistry of basalts generated in island arcs. Strongly negative Eu and Ce anomalies in metaultramafics indicate

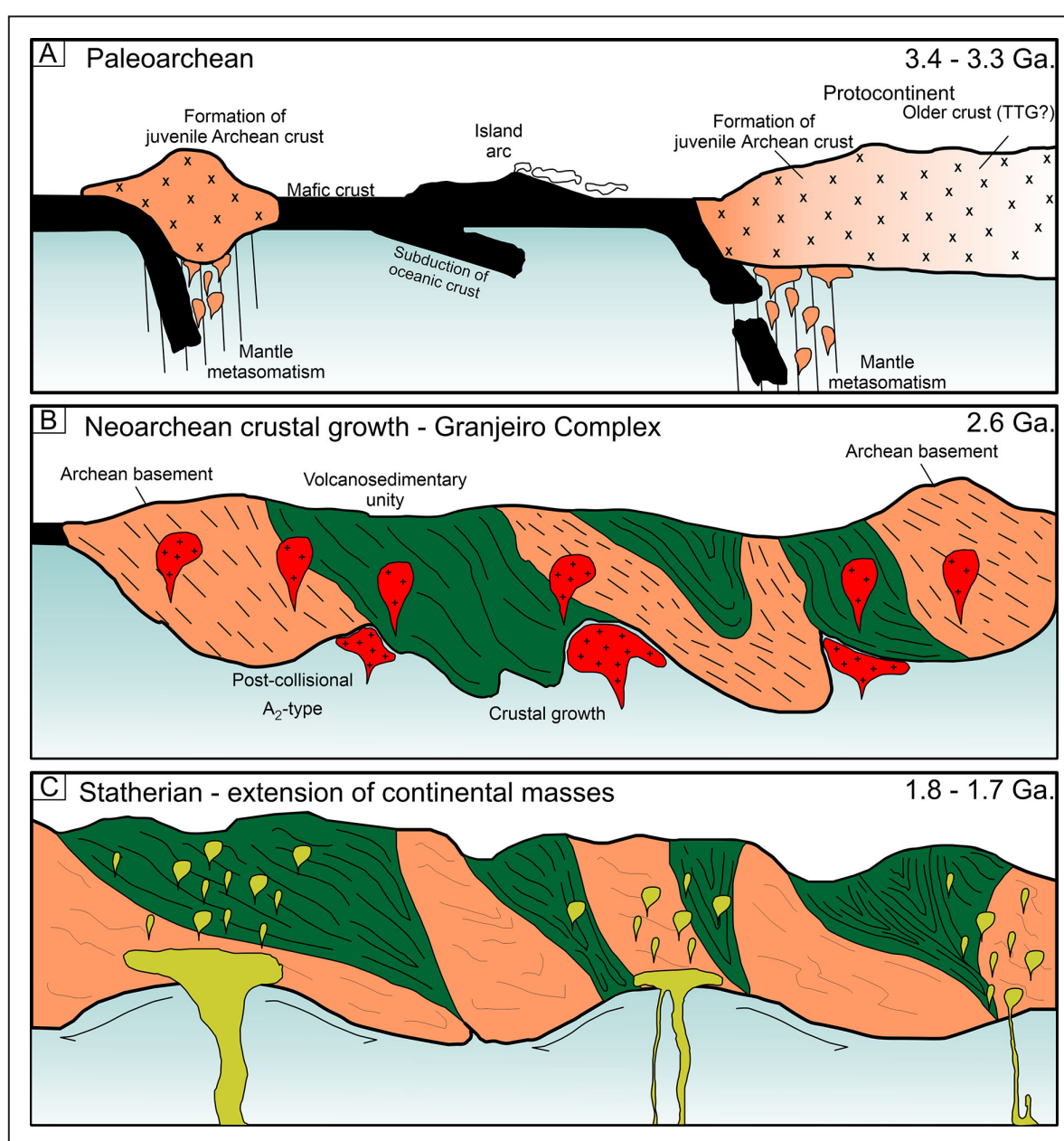


**FIGURE 18.** Schematic model of dynamic evolution of the Granjeiro Complex during the Archean-Paleoproterozoic: A) Generation of magma and formation of “island arcs” during the Paleoproterozoic; B) Neoproterozoic crustal growth with the crystallization of post-collisional syenogranitic to syenitic magmas of type A<sub>2</sub>; C) Extension of continental masses during the Statherian period and accommodation of pegmatite plutonic bodies.



a more primitive character than metamafic lithotypes and conditions associated with an oxidizing environment;

4 – Banded iron rocks show impoverishment of REE and slightly positive Eu anomalies indicate prevalence in chemical precipitation of low-temperature fluids;

5 – The lithotypes of the Granjeiro Complex were formed from a protocrust derived from the mantle, with the generation of more evolved rocks through accretion in magmatic arc environments;

6 – The existing syenogranitic orthogneisses aged ca. 2.6 Ga, an intrusive unit in the Paleoarchean gneisses, represents the end of a phase of regional crustal growth during the Archean. Its enrichment in LILE and HFSE elements, such as Rb, Th, Ta, Nb, Nd, Y and Yb resembles type A2 post-collisional granites;

7 – Orosirian orogenesis is well marked in the rocks of the Granjeiro Complex, with pre-existing ages derived from zircons formed and inherited from ca. 2.20 to 1.94 Ga that characterize the event of regional crustal deformation and high metamorphism that played a fundamental role in the consolidation of the Columbia supercontinent;

8 – The great extensional event of the Statherian period is present through the presence of pegmatite granitic bodies of ca. age. 1.75 Ga, which were responsible for local metasomatism;

9 – Although superimposed by the most recent deformation in the Neoproterozoic through shear zones, the metavolcano-sedimentary association rocks still preserve evidence of hydrothermal alteration, responsible for the reconcentration of iron and the formation of hydrothermal magnetite in banded iron rocks, carbonate alteration and quartz veins;

10 – Sulfur isotopes arising from pyrite crystals in veins that cut metamafic rocks indicate deep magmatic sources. The sulfur was probably derived from magmatic fluids or inherent in the host rocks due to fluid-rock interaction processes.

## Acknowledgments

This work received support from the Geological Survey of Brazil (SGB), through the project “Faixas Marginais da Borda Noroeste do Craton do São Francisco – Área Faixa riacho do Pontal”. The authors would like to thank the company Bemisa Mineração e Logística SA, for kindly providing drilling cores for description and collection of geological data. This article was improved following comments and suggestions from reviewers Dr. Paulo Gorayeb and Dr. Guilherme Teles, as well as the magazine's editor, Dr. Evandro Klein.

## Authorship credits

Author	A	B	C	D	E	F
JARV						
LVSM						
CFB						
VCM						
DAS						
ECUF						
NCPJ						
JBR						
TJSS						

A - Study design/Conceptualization B - Investigation/Data acquisition  
C - Data Interpretation/ Validation D - Writing  
E - Review/Editing F - Supervision/Project administration

## Appendices

Appendix 1. Table with chemical analysis of major elements (wt. %) and traces (ppm) of the granodioritic to tonalitic orthogneisses of the Granjeiro Complex.

Appendix 2. Table with chemical analysis of major elements (wt. %) and traces (ppm) of the syenogranitic to syenitic orthogneisses of the Granjeiro Complex.

Appendix 3. Table with chemical analysis of major elements (wt. %) and traces (ppm) of the metamafic rocks of the Granjeiro Complex.

Appendix 4. Table with chemical analysis of major elements (wt. %) and traces (ppm) of the metaultramafic rocks of the Granjeiro Complex.

Appendix 5. Table with chemical analysis of major elements (wt. %) and traces (ppm) of the banded iron rocks of the Granjeiro Complex.

Appendix 6. Summary of LA-ICP-MS data of zircons from the migmatitic orthogneiss sample (CB-03).

Appendix 7. Summary of LA-ICP-MS data of zircons from the sinogranitic orthogneiss sample (JR-333).

Appendix 8. Summary of LA-ICP-MS data of zircons from the amphibolite sample (DS-07).

Appendix 9. Summary of LA-ICP-MS data of zircons from the pegmatite intrusive body sample (JR-289A).

## References

- Albarède, F. 2009. *Geochemistry: an introduction*. 2nd edition. Cambridge University Press, 356 p.
- Alexander B.W., Bau M., Andersson P., Dulski P. 2008. Continentially derived solutes in shallow Archean seawater: rare earth element and Nd isotope evidence in iron formation from the 2.9 Ga Pongola Supergroup, South Africa". *Geochimica et Cosmochimica Acta*, 72, 378-394. <https://doi.org/10.1016/j.gca.2007.10.028>
- Almeida F.F.M., Hasui Y., Brito Neves B.B., Fuck R.A. 1981. Brazilian structural provinces: an introduction. *Earth-Science Reviews*, 17(1-2), 1-29. [https://doi.org/10.1016/0012-8252\(81\)90003-9](https://doi.org/10.1016/0012-8252(81)90003-9)
- Ancelmi M.F. 2016. *Geocronologia e geoquímica das rochas arqueanas do Complexo Granjeiro, Província Borborema*. PhD Thesis, Instituto de Geociências, Universidade Estadual de Campinas, Campinas, 159 p. <https://doi.org/10.47749/T/UNICAMP.2016.979098>
- Angelim L.A.A., Vasconcelos A.M., Gomes J.R.C., Wanderley A.A., Forgiarini L.L., Medeiros M.F. 2004. Folhas SB.24-Jaguaribe. In: Schobbenhaus C. Gonçalves J.H. Santos J.O.S., Abram M.B., Leão Neto R., Matos G.M.M., Vidotti R.M., Ramos M.A.B. Jesus J.D.A. Carta geológica do Brasil ao milionésimo: Jaguaribe: folha SB.24. Programa Geologia do Brasil. Brasília, CPRM. Escala 1:1.000.000. Available online at: <https://rigeo.sgb.gov.br/handle/doc/4978/> (accessed on 27 March 2023).
- Araujo C.E.G., Cordani U.G., Basei M.A.S., Castro N.A., Sato K., Sproesser W.M. 2012. U–Pb detrital zircon provenance of metasedimentary rocks from the Ceará Central and Médio Coreau Domains, Borborema Province, NE-Brazil: tectonic implications for a long-lived Neoproterozoic active continental margin. *Precambrian Research*, 206-207, 36-51. <https://doi.org/10.1016/j.precamres.2012.02.021>
- Archanjo C. Hollanda M.H.B.M., Viegas G. 2021. Late Ediacaran lateral-escape tectonics as recorded by the Patos shear zone, NE Brazil. *Brazilian Journal of Geology*, 51(2), 5-28. <https://doi.org/10.1590/2317-488920210200132>
- Armstrong R.L. 1981. Radiogenic isotopes: the case for crustal Recycling on a near-steady-state no-continental-growth earth. *Mathematical and Physical Sciences*, 301(1461), 443-471. <https://doi.org/10.1098/rsta.1981.0122>
- Basta F.F., Maurice A.E., Fontboté L., Favarger P.Y. 2011. Petrology and geochemistry of the banded iron formation (BIF) of Wadi Karim and Um Anab, Eastern Desert, Egypt: implications for the origin of Neoproterozoic BIF. *Precambrian Research*, 187(3-4), 277-292. <https://doi.org/10.1016/j.precamres.2011.03.011>
- Bau M. 1993. Effects of syn- and post-depositional processes on the rare-earth element distribution in Precambrian iron-formations. *European Journal of Mineralogy*, 5(2), 257-268. <https://doi.org/10.1127/ejm/5/2/0257>
- Bau M., Möller P. 1993. Rare earth element systematics of the chemically precipitated component in early Precambrian iron formations and the evolution of the terrestrial atmosphere-hydrosphere-lythosphere system. *Geochimica et Cosmochimica Acta*, 57(10), 2239-2249. [https://doi.org/10.1016/0016-7037\(93\)90566-F](https://doi.org/10.1016/0016-7037(93)90566-F)

- Bautista J.M.R. 2012. Estudo de proveniência sedimentar de seqüências neoproterozóicas ao longo do lineamento Patos (Província Borborema, NE do Brasil). MSc Dissertation, Instituto de Geociências, Universidade de São Paulo, São Paulo, 111 p. Available online at: <https://doi.org/10.11606/D.44.2012.tde-12062015-093701> / (accessed on 28 March 2023).
- Bédard J.H. 2006. A catalytic delamination-driven model for coupled genesis of Archaean crust and sub-continental lithospheric mantle. *Geochimica et Cosmochimica Acta*, 70(5), 1188-1214. <https://doi.org/10.1016/j.gca.2005.11.008>
- Belousova E.A., Kostitsyn Y.A., Griffin W.L., Begg G.C., O'Reilly S.Y., Pearson N.J. 2010. The growth of the continental crust: Constraints from zircon HF-isotope data. *Lithos*, 119(3-4), 457-466. <https://doi.org/10.1016/j.lithos.2010.07.024>
- Best M.G. 2003. *Igneous and metamorphic petrology*. 2nd edition. Oxford Blackwell Science, 729 p.
- Bleeker W. 2003. The late Archean record: a puzzle in ca. 35 pieces. *Lithos*, 71(2-4), 99-134. <https://doi.org/10.1016/j.lithos.2003.07.003>
- Bolhar R., Kamber B.S., Moorbath S., Fedo C.M., Whitehouse M.J. 2004. Characterisation of early Archaean chemical sediments by trace element signatures. *Earth and Planetary Science Letters*, 222(1), 43-60. <https://doi.org/10.1016/j.epsl.2004.02.016>
- Boynton W.V. 1984. Cosmochemistry of the rare earth element: meteorite studies. In: Henderson P. (ed.). *Rare earth element geochemistry*. Amsterdam, Elsevier, 63-114. <https://doi.org/10.1016/B978-0-444-42148-7.50008-3>
- Brito Neves B.B., Sá Z.M., Nilson A.A., Botelho N.F. 1995. A tafrogênese estateriana nos blocos paleoproterozoicos da América do Sul e processos subsequentes. *Geonomos*, 3(2), 1-21. <https://doi.org/10.18285/geonomos.v3i2.205>
- Brito Neves B.B., Santos E.J., Van Schmus W.R. 2000. Tectonic history of the Borborema Province. In: Cordani U.G., Milani E.J., Thomaz Filho A., Almeida D.A. (eds.). *Tectonic evolution of South America*. Rio de Janeiro, 31th International Geological Congress, 151-182. Available online at: <https://rigeo.sgb.gov.br/handle/doc/19419>
- Brito Neves B.B., Santos T.J.S., Dantas E.L. 2022. O terreno tectonoestratigráfico São Pedro: Oeste da Zona Transversal – Província Borborema. *Geologia USP Série científica*, 22(4), 45-69. <https://doi.org/10.11606/issn.2316-9095.v22-197489>
- Brown M. 1973. The definition of metatexis, diatexis and migmatite. *Proceedings of the Geologists' Association*, 84(4), 371-382. [https://doi.org/10.1016/S0016-7878\(73\)80021-5](https://doi.org/10.1016/S0016-7878(73)80021-5)
- Calado B.O., Costa F.G., Gomes I.P., Rodrigues J.B. 2019. Evidence for ca. 2046 Ma high-grade metamorphism in Paleoproterozoic metasedimentary rocks of the northern Borborema Province, NE Brazil: constraints from U-Pb (LA-ICP-MS) zircon ages. *Journal of the Geological Survey of Brazil*, 2(3), 137-150. <https://doi.org/10.29396/jgsb.2019.v2.n3.1>
- Campos M., Braga A.P.G., Sousa E.M., Silva F.A.F., França J.F. 1976. Projeto Rio Jaguaribe: relatório final. Recife, DNPM, CPRM. Available online at: <https://rigeo.sgb.gov.br/handle/doc/9327> / (accessed on 27 March 2023).
- Cavalcante J.C. 1999. Limites e evolução geodinâmica do sistema Jaguaribeano, Província Borborema, Nordeste do Brasil. MSc Dissertation, Universidade Federal do Rio Grande do Norte, Natal, 183 p. Available online at: <https://repositorio.ufrn.br/jspui/handle/123456789/18735> / (accessed on 25 October 2023).
- Cavalcante R., Medeiros V.C., Costa A.P., Sá J.M., Santos R.V., Rodrigues J.B., Dantas A.R., Nascimento M.A.L., Cunha A.L.C. 2018. Neoproterozoic, Rhyacian and Neoproterozoic units of the Saquinho region, eastern Rio Piranhas-Seridó domain, Borborema Province (northeastern Brazil): implications for the stratigraphic model. *Journal of the Geological Survey of Brazil*, 1(1), 11-29. <https://doi.org/10.29396/jgsb.2018.v1.n1.2>
- Caxito F.A., Basto C.F., Santos L.C.M.L., Dantas E.L., Medeiros V.C., Dias T.G., Barrote V., Hagemann S., Alkimim A.R., Lana C. 2021. Neoproterozoic magmatic arc volcanism in the Borborema Province, NE Brazil: possible flare-ups and lulls and implications for western Gondwana assembly. *Gondwana Research*, 92, 1-25. <https://doi.org/10.1016/j.gr.2020.11.015>
- Cawood P.A., Hawkesworth C.J., Dhuime B. 2013. The continental record and the generation of continental crust. *Geological Society of America Bulletin*, 125(1-2), 14-32. <https://doi.org/10.1130/B30722.1>
- Chaussidon M., Lorand J.P. 1990. Sulphur isotope composition of orogenic spinel Iherzolite massifs from Ariège (North-Eastern Pyrenees, France): An ion microprobe study. *Geochimica et Cosmochimica Acta*, 54(10), 2835-2846. [https://doi.org/10.1016/0016-7037\(90\)90018-G](https://doi.org/10.1016/0016-7037(90)90018-G)
- Condie K.C. (ed.). 1981. *Archaean greenstone belts*. Developments in Precambrian Geology, 3. Amsterdam, Elsevier, 395 p.
- Condie K.C., Kroner A. 2013. The building blocks of the continental crust: evidence for a major change in the tectonic setting of continental growth at the end of the Archean. *Gondwana Research*, 23(2), 394-402. <https://doi.org/10.1016/j.gr.2011.09.011>
- Condie K.C., O'Neill C. 2010. The Archaean-Proterozoic boundary: 500 My of tectonic transition in Earth history. *American Journal of Science*, 310(9), 775-790. <https://doi.org/10.2475/09.2010.01>
- Craddock P.R., Rouxel O.J., Ball L.A., Bach W. 2008. Sulfur isotope measurement of sulfate and sulfide by high-resolution MC-ICP-MS. *Chemical Geology*, 253(3-4), 102-113. <https://doi.org/10.1016/j.chemgeo.2008.04.017>
- Dantas A.R., Cavalcante R., Costa A.P., Cunha A.L.C., Lages G.A., Spisila A.L., Rodrigues J.B. 2019. Unidades arqueanas na porção norte da Faixa Seridó – Corpo Máfico Serra do Ingá e Complexo Amarante. In: Simpósio de Geologia do Nordeste, 28, 482. Available online at: [http://sbgeo.org.br/assets/admin/imgCk/files/Anais/Anais\\_28o\\_Simpósio\\_de\\_Geologia\\_do\\_Nordeste-ISBN.pdf](http://sbgeo.org.br/assets/admin/imgCk/files/Anais/Anais_28o_Simpósio_de_Geologia_do_Nordeste-ISBN.pdf) / (accessed on 31 March 2023).
- Dantas E.L., Van Schmus W.R., Hackspacher P.C., Fetter A.H., Brito Neves B.B., Cordani U., Nutman A.P., Williams I.S. 2004. The 3.5-3.4 Ga São José do Campestre massif, NE Brazil: remnants of the oldest crust in South America. *Precambrian Research*, 130(1-4), 113-137. <https://doi.org/10.1016/j.precamres.2003.11.002>
- Dantas E.L., Zorano S.S., Wernick E., Hackspacher P.C., Martin H., Xiaodong D., Li J.W. 2013. Crustal growth in the 3.4-2.7 Ga São José do Campestre Massif, Borborema Province, NE Brazil. *Precambrian Research*, 227, 120-156. <https://doi.org/10.1016/j.precamres.2012.08.006>
- Delgado I.M., Souza J.D., Silva L.C., Silveira Filho N.C., Santos R.A., Pedreira A.J., Guimarães J.T., Angelim L.A.A., Vasconcelos A.M., Gomes I.P., Lacerda Filho J.V., Valente C.R., Perrotta M.M., Heineck C.A. 2003. Geotectônica do Escudo atlântico. In: Bizzi L.A., Schobbenhaus C., Vidotti R.M., Gonçalves J.H. *Geologia, tectônica e recursos minerais do Brasil: texto, mapas e SIG*. Brasília, CPRM, 227-334. Available online at: <https://rigeo.sgb.gov.br/handle/doc/5006> / (accessed on 31 March 2023).
- Dhuime B., Hawkesworth C.J., Cawood P.A., Storey C.D. 2012. A change in the geodynamics of continental growth 3 billions years ago. *Science*, 335(1674), 1334-1336. <https://doi.org/10.1126/science.1216066>
- Eby G.N. 1992. Chemical subdivision of the A-type granitoids: petrogenetic and tectonic implications. *Geology*, 20(7) 641-644. [https://doi.org/10.1130/0091-7613\(1992\)020<0641:CSOTAT>2.3.CO;2](https://doi.org/10.1130/0091-7613(1992)020<0641:CSOTAT>2.3.CO;2)
- Elderfield H., Upstill-Goddard R., Sholkovitz E.R. 1990. The rare earth elements in rivers, estuaries, and coastal seas and their significance to the composition of ocean waters. *Geochimica et Cosmochimica Acta*, 54(4), 971-991. [https://doi.org/10.1016/0016-7037\(90\)90432-K](https://doi.org/10.1016/0016-7037(90)90432-K)
- Ferreira A.C.D., Dantas E.L., Fuck R.A., Nedel I.M. 2020. Arc accretion and crustal reworking from late Archean to Neoproterozoic in Northeast Brazil. *Scientific Reports*, 10, 7855. <https://doi.org/10.1038/s41598-020-64688-9>
- Fetter A.H. 1999. U-Pb and Sm-Nd geochronological constraints on the crustal framework and geologic history of Ceará state, NW Borborema province, NE Brazil: implications for the Assembly of Gondwana. PhD Thesis, Department of Geology, University of Kansas, Kansas, 164 p.
- Floyd P.A., Winchester J.A. 1975. Magma type and tectonic setting discrimination using immobile elements. *Earth and Planetary Science Letters*, 27(2), 211-218. [https://doi.org/10.1016/0012-821X\(75\)90031-X](https://doi.org/10.1016/0012-821X(75)90031-X)
- Foley S., Tiepolo M., Vanucci R. 2002. Growth of early continental crust controlled by melting of amphibolite in subduction zones. *Nature*, 417(6891), 837-840. <https://doi.org/10.1038/nature00799>
- Frei R., Dahl P.S., Duke E.F., Frei K.M., Hansen T.R., Frandsson M.M., Jensen L.A. 2008. Trace element and isotopic characterization of Neoproterozoic and Paleoproterozoic iron formations in the Black Hills (South Dakota, USA): assessment of chemical change during 2.9–1.9 Ga deposition bracketing the 2.4–2.2 Ga first rise of atmospheric oxygen. *Precambrian Research*, 162(3-4), 441-474. <https://doi.org/10.1016/j.precamres.2007.10.005>
- Freimann M.A. 2014. Geocronologia e petrografia de quartzito milonitos do duplex transcorrente de Lavras da Mangabeira. MSc Dissertation, Instituto de Geociências, Universidade de São Paulo, São Paulo, 83 p. <https://doi.org/10.11606/D.44.2014.tde-26112014-144455>
- Friend C.R.L., Nutman A.P. 2005. Complex 3670-3500 Ma Orogenic Episodes Superimposed on Juvenile Crust Accreted between 3850



- and 3690 Ma, Itsaq Gneiss Complex, Southern West Greenland. *The Journal of Geology*, 113(4), 375-397. <https://doi.org/10.1086/430239>
- Frost B.R., Barnes C.G., Collins W.J., Arculus R.J., Ellis D.J., Frost, C.D. 2001. A geochemical classification for granitic rocks. *Journal of Petrology*, 42(11), 2033-2048. <https://doi.org/10.1093/ptetrology/42.11.2033>
- Ganade C.E., Basei M.A.S., Grandjean F.C., Armstrong R., Brito R.S. 2017. Contrasting Archean (2.85-2.68 Ga) TTGs from the Tróia Massif (NE-Brazil) and their geodynamic implications for flat to steep subduction transition. *Precambrian Research*, 297, 1-18. <https://doi.org/10.1016/j.precamres.2017.05.007>
- Garcia M.G.M., Santos T.J.S., Amaral W.S. 2014. Provenance and tectonic setting of neoproterozoic supracrustal rocks from the Ceará Central Domain, Borborema Province (NE Brazil): constraints from geochemistry and detrital zircon ages. *International Geology Review*, 56(4), 481-500. <https://doi.org/10.1080/00206814.2013.875489>
- Gill, R. 2010. *Igneous rocks and process: a practical guide*. 2nd edition. Wiley, 496 p.
- Gomes E.N. 2013. *Protominérios e minérios de manganês de Juá – CE*. MSc Dissertation, Departamento de Geologia, Universidade Federal do Ceará, Fortaleza, 107 p. Available online at: <http://www.repositorio.ufc.br/handle/riufc/16909> / (accessed on 29 March 2023).
- Gomes I.P., Palheta E.S.M., Braga I.F., Costa F.G., Souza F.R.F.R.O., Rocha J.M.A., Freire D.P.C., Holanda J.L.R. 2021. Projeto mapeamento geológico e integração geológica-geofísica-geoquímica na região de Granjeiro-Cococi, Ceará. Programa Geologia, Mineração e Transformação Mineral. Fortaleza, CPRM. 175 p. Available online at: <https://rigeo.sgb.gov.br/handle/doc/18691> / (accessed on 30 March 2023).
- Gomes J.R.C., Vasconcelos A.M. 2000. Jaguaribe SW: folha SB.24-Y: estados do Ceará, Pernambuco e Piauí. Escala 1:500.000. Geologia e Metalogênese. Programa Levantamentos Geológicos Básicos do Brasil. Brasília, CPRM, 103 p. Available online at: <https://rigeo.sgb.gov.br/handle/doc/5362> / (accessed on 21 December 2022).
- Grebennikov A.V. 2014. A-type granites and related rocks: petrogenesis and classification. *Russian Geology and Geophysics*, 55(9), 1074-1086. <https://doi.org/10.1016/j.rgg.2014.08.003>
- Irvine T.N., Baragar W.R.A. 1971. A guide to the chemical classification of the common volcanic rocks. *Canadian Journal of the Earth Sciences*, 8(5), 523-548. <https://doi.org/10.1139/e71-055>
- Jackson S.E., Pearson N.J., Griffin W.L., Belousova E.A. 2004. The application of laser ablation-inductively coupled plasma-mass spectrometry to in situ U–Pb zircon geochronology. *Chemical Geology*, 211(1-2), 47-69. <https://doi.org/10.1016/j.chemgeo.2004.06.017>
- Jardim de Sá E.F. 1994. A Faixa Seridó (Província Borborema, NE do Brasil) e o seu significado geodinâmico na Cadeia Brasileira/Pan-Africana. PhD Thesis, Instituto de Geociências, Universidade de Brasília, Brasília, 803 p.
- Jensen L.S. 1976. A New cation plot for classifying subalkalic volcanic rocks. *Miscellaneous Paper*, 66. Ontario Division Mines, 22 p. Available online at: <http://www.geologyontario.mndmf.gov.on.ca/mndmfiles/pub/data/imaging/MP066/MP066.pdf> / (accessed on 28 March 2023).
- Jesus B.A. 2011. Rochas máficas e ultramáficas do Complexo Riacho da Telha, Maciço São José do Campeste, Província Borborema, NE do Brasil. MSc Dissertation, Instituto de Geociências, Universidade de Brasília, Brasília, 80 p. Available online at: <https://repositorio.unb.br/handle/10482/9364> / (accessed on 31 March 2023).
- Kato Y., Kano T., Kunugiza K. 2002. Negative Ce Anomaly in the Indian banded iron formations: evidence for the emergence of oxygenated deep-sea at 2.9-2.7 Ga. *Resource Geology*, 52(2), 101-110. <https://doi.org/10.1111/j.1751-3928.2002.tb00123.x>
- Kato Y., Yamaguchi K.E., Ohmoto H. 2006. Rare earth elements in Precambrian banded iron formations: secular changes of Ce e Eu anomalies and evolution of atmospheric oxygen. In: Kesler S.E., Ohmoto H. (eds.). *Evolution of Early earth's atmosphere, hydrosphere, and biosphere: constraints from ore deposits*. Memoir of Geological Society of America, 198. Geological Society of America. p. 269-289. [https://doi.org/10.1130/2006.1198\(16\)](https://doi.org/10.1130/2006.1198(16))
- Kearey P., Klepeis K.A., Vine F.J. 2009. *Global tectonics*. 3rd. edition, Wiley-Blackwell, 482 p.
- Keller C.B., Schoene B. 2012. Statistical geochemistry reveals disruption in secular lithospheric evolution about 2.5 Gyr ago. *Nature*, 485, 490-493. <https://doi.org/10.1038/nature11024>
- Lana C., Farina F., Gerdes A., Alkmim A., Gonçalves G.O., Jardim A.C. 2017. Characterization of zircon reference materials via high precision U–Pb LA-ICP-MS. *Journal of Analytical Spectroscopy*, 32, 2011-2023. <https://doi.org/10.1039/c7ja00167c>
- Laurent O., Martin H., Moyen J.F., Doucelance R. 2014. The diversity and evolution of late-Archean granitoids: evidence for the onset of "modern-style" plate tectonics between 3.0 and 2.5 Ga. *Lithos*, 205, 208-235. <https://doi.org/10.1016/j.lithos.2014.06.012>
- Ludwig K.R. 2009. *Isoplot: a geochronological toolkit for Microsoft Excell*. Berkeley Geochronological Center Special Publication, 2, 17.
- Martin H. 1994. The Archean grey gneisses and the genesis of continental crust. In: *Condie K.C. Archean Crustal Evolution*. Developments in Precambrian Geology, 11. Amsterdam, Elsevier, p. 205-260. [https://doi.org/10.1016/S0166-2635\(08\)70224-X](https://doi.org/10.1016/S0166-2635(08)70224-X)
- Martins D.T. 2017. *Geologia do terreno arqueano Granjeiro (3.4 a 2.6 Ga), Província Borborema*. MSc Dissertation, Departamento de Geologia, Universidade Federal do Ceará, Fortaleza, 53 p. Available online at: <http://www.repositorio.ufc.br/handle/riufc/26573> / (accessed on 29 March 2023).
- McDonough W.F., Sun S.S. 1995. The composition of the Earth. *Chemical Geology*, 120(3-4), 223-253. [https://doi.org/10.1016/0009-2541\(94\)00140-4](https://doi.org/10.1016/0009-2541(94)00140-4)
- Medeiros V.C., Cavalcante R., Santos F.G., Rodrigues J.B., Santana J.S., Costa A.P., Neto I.C. 2021. The Rio Piranhas-Seridó Domain, Borborema Province, Northeastern Brazil: review of geological-geochronological data and implications for stratigraphy and crustal evolution. *Journal of the Geological Survey of Brazil*, 4(3), 179-207. <https://doi.org/10.29396/jgsb.2021.v4.n3.1>
- Moyen J.F. 2011. The composite Archean grey gneisses: petrological significance, and evidence for a non-unique tectonic setting for Archean crustal growth. *Lithos*, 123(1-4), 21-36. <https://doi.org/10.1016/j.lithos.2010.09.015>
- Moyen J.F., Martin H. 2012. Forty years of TTG research. *Lithos*, 148, 312-336. <https://doi.org/10.1016/j.lithos.2012.06.010>
- Moyen J.F., Stevens G. 2006. Experimental constraints on TTG Petrogenesis: implications for archean geodynamics. In: *Benn K., Mareschal J.C., Condie K.C. Archean geodynamics and environments*. Geophysical Monograph Series, 164. Washington D.C., American Geophysical Union, 149-175. <https://doi.org/10.1029/164GM11>
- Mullen E.D. 1983. MnO/TiO<sub>2</sub>/P<sub>2</sub>O<sub>5</sub>: a minor element discriminant for basaltic rocks of oceanic environments and its implications for petrogenesis. *Earth and Planetary Science Letters*, 62(1), 53-62. [https://doi.org/10.1016/0012-821X\(83\)90070-5](https://doi.org/10.1016/0012-821X(83)90070-5)
- Muniz R.L., Santos T.J.S., Dantas E.L., Fuck R.A. 2022. Rhyacian-Orosirian khindalite belt in the Borborema Province (NE Brazil): an active margin setting based on U–Pb zircon and monazite constrains. *Geological Journal*, 57(9), 3808-3828. <https://doi.org/10.1002/gj.4517>
- Neves S.P., Bruguier O., Vauchez A., Bosh D., Silva J.M.R., Mariano G. 2006. Timing of crust formation, deposition of supracrustal sequences, and Transamazonian and Brasiliano metamorphism in the East Pernambuco belt (Borborema Province, NE Brazil): implications for western Gondwana assembly. *Precambrian Research*, 149(3-4), 197-216. <https://doi.org/10.1016/j.precamres.2006.06.005>
- Ohmoto H., Rye R.O. 1979. Isotopes of sulfur and carbon. In: *Barnes H.L. Geochemistry of hydrothermal ore deposits*. New York, Wiley, 992 p.
- Oliveira R.G., Domingos, N.R.R., Medeiros W.E. 2023. Deep crustal structure of the Sergipano Belt, NE-Brazil, revealed by integrated modeling of gravity, magnetic, and geological data. *Journal of the Geological Survey of Brazil* 6(1),1-22. <https://doi.org/10.29396/jgsb.2023.v6.n1.1>
- Paton C., Woodhead J.D., Hellstrom J.C., Hergt J.M., Greig A., Maas R. 2010. Improved laser ablation U–Pb zircon geochronology through robust downhole fractionation correction. *Geochronology, Geophysics, Geosystems*, 11, 1-36. <https://doi.org/10.1029/2009GC002618>
- Pearce J.A. 1996. Source and settings of granitic rocks. *Episodes*, 19(4), 120-125. <https://doi.org/10.18814/epiugs/1996/v19i4/005>
- Pearce T.H., Gorman B.E., Birkett T.C. 1977. The relationship between major element chemistry and tectonic environment of basic and intermediate volcanic rocks. *Earth and Planetary Science Letters*, 36(1), 121-132. [https://doi.org/10.1016/0012-821X\(77\)90193-5](https://doi.org/10.1016/0012-821X(77)90193-5)
- Pecoits E., Gingras M.K., Barley M.E., Kappler A., Posth N.R., Konhauser K.O. 2009. Petrography and geochemistry of the Dales Gorge banded iron formation: Paragenetic sequence, source and implications for palaeo-ocean chemistry. *Precambrian Research*, 172(1-2), 163-187. <https://doi.org/10.1016/j.precamres.2009.03.014>
- Percival J.A. 1994. Archean high-grade metamorphism. *Developments in Precambrian Geology*, 11. Amsterdam, Elsevier, p. 357-410. [https://doi.org/10.1016/S0166-2635\(08\)70227-5](https://doi.org/10.1016/S0166-2635(08)70227-5)

- Petrus J.A., Kamber B.S. 2012. VizualAge: a novel approach to laser ablation ICP-MS U-Pb geochronology data reduction. *Geostandards and Geoanalytical Research*, 36(3), 247-270. <https://doi.org/10.1111/j.1751-908X.2012.00158.x>
- Pinéo T.R.G., Costa F.G., Basto C.F., Rodrigues J.B., Medeiros V.C., Palheta E.S.M., Calado B.O., Cavalcante R., Mesquita R.B., Santos F.G., Brasilino R.G., Dantas A.R., Morais D.M.F., Santana J.S. 2023. New zircon U-Pb dating and review of geological and geochronological data with implications for lithostratigraphy and crustal evolution of North Borborema Province, northeastern Brazil. *Journal of the Geological Survey of Brazil*, 6(1), 23-41. <https://doi.org/10.29396/jgsb.2023.v6.n1.3>
- Pitarello M.Z., Santos T.J.S., Ancelmi W.F. 2019. Syn-to Post-depositional processes related to high grade metamorphic BIFs: geochemical and geochronological evidences from a Paleo to Neoproterozoic (3.5 to 2.6 Ga) terrane in NE Brazil. *Journal of South American Earth Sciences*, 96, 102312. <https://doi.org/10.1016/j.jsames.2019.102312>
- Prado F.S., Oliveira A.A., Leite E.A., Gomes F.E.M., Silva F.P., Colares J.Q.S. 1980. Projeto Lavras de Mangabeira: relatório da etapa I. Fortaleza, DNPM, CPRM. Available online at: <https://rigeo.sgb.gov.br/handle/doc/8146> / (accessed on 28 March 2023).
- Rapp R.P., Shimizu N., Norman M.D. 2003. Growth of early continental crust by partial melt of eclogite. *Nature*, 425(6958), 605-609. <https://doi.org/10.1038/nature02031>
- Ribeiro J.A., Vasconcelos A.M. 1991. Simões, folha SB.24-Y-C-VI. Programa Levantamentos Geológicos Básicos do Brasil. Brasília, DNPM, CPRM, 135p. Available on line at: <https://rigeo.sgb.gov.br/handle/doc/8501> / (accessed on 19 October 2023).
- Ruiz F.V., Giustina M.E.S.D., Oliveira C.G., Dantas E.L., Hollanda M.H.B. 2019. The 3.5 Ga São Tomé layered mafic-ultramafic intrusion, NE Brazil: insights into a Paleoproterozoic Fe-Ti-V oxide mineralization and its reworking during West Gondwana assembly. *Precambrian Research*, 326, 462-478. <https://doi.org/10.1016/j.precamres.2018.03.011>
- Sá J.M., Souza L.C., Legrand J.M., Galindo A.C., Maia H.N., Fillippi R.R. 2014. U-Pb and Sm-Nd data of the Rhyacian and Statherian Orthogneisses from Rio Piranhas-Seridó and Jaguaribeano Terranes, Borborema Province, Northeast of Brazil. *Geologia USP, Série Científica*, 14 (3), 97-110. <https://doi.org/10.5327/Z1519-874X201400030007>
- Santos E.J., Souza Neto J.A., Silva M.M.R., Beurlen H., Cavalcanti J.A.D., Silva M.G., Costa A.F., Santos L.C.M.L., Santos R.B. 2014. Metalogênese das porções norte e central da Província Borborema. In: Silva M.G., Rocha Neto M.B., Jost H., Kuyumjian R.M. Metalogênese das províncias tectônicas brasileiras. Belo Horizonte, CPRM, p. 343-388. Available on line at: <https://rigeo.sgb.gov.br/handle/doc/19389> / (accessed on 29 March 2023).
- Santos F.G., Cavalcanti Neto M.T.O., Ferreira V.P., Bertotti A.L. 2020. Eo to Paleoproterozoic metamafic-ultramafic rocks from the central portion of the Rio Grande do Norte Domain, Borborema Province, northeast Brazil: the oldest South American platform rock. *Journal of South American Earth Sciences*, 97, 102410. <https://doi.org/10.1016/j.jsames.2019.102410>
- Santos F.G., Pinéo T.R.G., Medeiros V.C., Santana J.S., Morais D.M.F., Vale J.A.R., Wanderley A.A. Mapa geológico da Província Borborema. Projeto Geologia e Potencial Mineral da Província Borborema. Escala 1:1.000.000. Recife, CPRM, 2021. Available on line at: <https://rigeo.sgb.gov.br/handle/doc/22508> / (accessed on 29 March 2023).
- Santos M.M., Lana C., Scholz R., Buick I., Schmitz M.D., Kamo S.L., Gerdes A., Corfu F., Tapster S., Lancaster P., Storey C.D., Basei M.A.S., Tohver E., Alkmim A., Nalini H., Krambrock K., Fantini C., Wiedenbeck M. 2017. A new appraisal of Sri Lankan BB zircon as a reference material for LA-ICP-MS U-Pb geochronology and Lu-Hf isotope tracing. *Geostandards and Geoanalytical Research*, 41(3), 335-358. <https://doi.org/10.1111/ggr.12167>
- Silva L.C. 1993. Petrologia e evolução dos gnaisses de alto grau na Folha Iguatu-CE. Fortaleza, CPRM.
- Sato E.N. 2011. Proposta metodológica sobre dados de geofísica aeroportada na prospecção de minério de Fe: indicação de ambientes geológicos propícios e geração de mapas de probabilidade na região de Curral Novo do Piauí (PI). MSc Dissertation, Instituto de Geociências, Universidade de São Paulo, São Paulo, 69 p. <https://doi.org/10.11606/D.44.2011.tde-27072011-095630>
- Sato K., Basei M.A.S., Siga Junior O., Sproesser W.M., Passarelli C.R. 2008. Novas técnicas aplicadas ao método U-Pb no CPGeo - IGc/ USP: avanços na digestão química, espectrometria de massa (TIMS) e exemplos de aplicação integrada com SHRIMP. *Geologia USP, Série Científica*, 8(2), 77-99. <https://doi.org/10.5327/Z1519-874X2008000200006>
- Silva L.C., McNaughton N.J., Vasconcelos A.M., Gomes J.R.C., Fletcher I.R. 1997. U-Pb SHRIMP ages in Southern State of Ceará, Borborema Province, NE Brazil: TIG accretion and Proterozoic crustal 'reworking'. In: International Symposium on Granites and Associated Mineralizations, 2, 280-281.
- Sláma J., Košler J., Condon D.J., Crowley J.L., Gerdes A., Hancher J.M., Horstwood M.S.A., Morris G.A., Nasdala L., Norberg N., Schaltegger U., Schoene B., Tubrett M.N., Whitehouse M.J. 2008. Plešovice zircon: a new natural reference material for U-Pb and Hf isotopic microanalysis. *Chemical Geology*, 249(1-2), 1-35. <https://doi.org/10.1016/j.chemgeo.2007.11.005>
- Smithies R.H., Champion D.C. 2000. The Archaean High-Mg diorite suite: links to tonalite-trondhjemite-granodiorite magmatism and implications for early archaean crustal growth. *Journal of Petrology*, 41(12), 1653-1671. <https://doi.org/10.1093/petrology/41.12.1653>
- Souza Z.S., Kalsbeek F., Deng X.D., Frei R., Kokfelt T.F., Dantas E.L., Li J.W., Pimentel M.M., Galindo A.C. 2016. Generation of continental crust in the northern part of the Borborema Province, northeastern Brazil, from Archaean to Neoproterozoic. *Journal of South American Earth Sciences*, 68, 68-96. <https://doi.org/10.1016/j.jsames.2015.10.006>
- Taylor S.R., McLennan, S.M. 1985. The continental crust: its composition and evolution: an examination of the geochemical record preserved in sedimentary rocks. Oxford, Blackwell Scientific Publications, 312 p.
- Taylor S.R., McLennan, S.M. 1995. The geochemical evolution of the continental crust. *Reviews of Geophysics*, 33(2), 241-265. <https://doi.org/10.1029/95RG00262>
- Teixeira W., Oliveira E.P., Peng P., Dantas E.L., Hollanda M.H.B.M. 2017. U-Pb geochronology of the 2.0 Ga Itapeçerica graphite-rich supracrustal succession in the São Francisco Craton: tectonic matches with the North China Craton and paleogeographic inferences. *Precambrian Research*, 293, 91-111. <https://doi.org/10.1016/j.precamres.2017.02.021>
- Uchôa Filho E.C., Vale J.A.R., Basto C.F., Silveira D.A., Freitas M.S., Pedrosa Junior N.C. 2019. Mapa de integração geológico-geofísico da faixa Riacho do Pontal. Escala 1:250.000. Teresina, CPRM. Empreendimento Áreas de Relevante Interesse Mineral-ARIM. Available online at: <https://rigeo.sgb.gov.br/handle/doc/18671> / (accessed on 29 March 2023).
- Van Schmus W.R., Oliveira E.P., Silva Filho A., Toteu S.F., Penaye J., Guimarães I.P. 2008. Proterozoic links between the Borborema Province, NE Brazil, and the Central African Fold Belt. *Geological Society, Special Publications*, 294(1), 69-99. <https://doi.org/10.1144/SP294.5>
- Vasconcelos A.M., Gomes F.E.M. 1998. Iguatu: folha SB.24-Y-B: estado do Ceará. Programa Levantamentos Geológicos Básicos do Brasil. Brasília, CPRM, 107 p. Available online at: <https://rigeo.sgb.gov.br/handle/doc/8840> / (accessed on 29 March 2023).
- Whalen J.B., Currie K.L., Chappell B.W. 1987. A-type granites: geochemical characteristics, discrimination and petrogenesis. *Contributions to Mineralogy and Petrology*, 95(4), 407-419. <https://doi.org/10.1007/BF00402202>
- Whitney D.L., Evans B.W. 2010. Abbreviations for names of rock-forming minerals. *American Mineralogist*, 95, 185-187. <http://dx.doi.org/10.2138/am.2010.3371>
- Wiedenbeck M., Allé P., Corfu F., Griffin W.L., Meier M., Oberli F., Von Quadt A., Roddick J.C., Spiegel W. 1995. Three natural zircon standards for U-Th-Pb, Lu-Hf trace element and Re analyses. *Geostandards Newsletter*, 19(1), 1-23. <https://doi.org/10.1111/j.1751-908X.1995.tb00147.x>
- Willbold M., Hegner E., Stracke A., Rocholl A. 2009. Continental geochemical signatures in dacites from Iceland and implications for models of early Archaean crust formation. *Earth and Planetary Sciences Letters*, 279(1-2), 44-52. <https://doi.org/10.1016/j.epsl.2008.12.029>
- Windley B.F. 1984. The Archaean-Proterozoic boundary. *Tectonophysics*, 105(1-4), 43-53. [https://doi.org/10.1016/0040-1951\(84\)90193-8](https://doi.org/10.1016/0040-1951(84)90193-8)
- Zhai M., Kampuzi A.B., Modisi M.P., Bagai Z. 2006. Sr and Nd isotope systematics of Francistown plutonic rocks, Botswana: implication for Neoproterozoic crustal evolution of the Zimbabwe craton. *International Journal of Earth Sciences*, 95, 355-369. <https://doi.org/10.1007/s00531-005-0054-6>
- Zhao G., Cawood P.A., Wilde S.A., Sun M. 2002. Review of global 2.1-1.8 orogens: implications for a pre-Rodinia supercontinent. *Earth-Science Reviews*, 59(1-4), 125-162. [https://doi.org/10.1016/S0012-8252\(02\)00073-9](https://doi.org/10.1016/S0012-8252(02)00073-9)